Tudor domain containing 12 (TDRD12) is essential for secondary piRNA biogenesis in mice

Radha Raman Pandey[a,b,1], Yoshimi Tokuzawa[c,1], Zhaolin Yang[a,b], Eri Hayashi[d,e], Tomoko Ichisaka[f], Shimpei Kajita[h], Yuka Asano[h], Tetsuo Kunieda[h], Ravi Sachidanandam[i], Shinichiro Chuma[d,e], Shinya Yamanaka[f,g,2] and Ramesh S. Pillai[a,b,2]

[a]European Molecular Biology Laboratory, Grenoble Outstation. [b]Unit for Virus Host-Cell Interactions, Univ. Grenoble Alpes-EMBL-CNRS, 6 rue Jules Horowitz, 38042 France.
[c]Division of Functional Genomics & Systems Medicine, Research Center for Genomic Medicine Saitama Medical University, Saitama 350-1241, Japan
[d]Institute for Frontier Medical Sciences and [e]Institute for Integrated Cell-Material Sciences, Kyoto University, Kyoto 606-8507, Japan.
[f]Center for iPS Cell Research and Application (CiRA), Kyoto University, Kyoto, 606-8507 Japan.
[g]Gladstone Institute of Cardiovascular Disease, San Francisco, CA 94158, USA
[h]Graduate School of Natural Science and Technology, Okayama University, Okayama 700-8530, Japan.
[i]Department of Genetics and Genomic Sciences, Mount Sinai School of Medicine, New York, NY 10029.

Running title: Mouse TDRD12 and secondary piRNA biogenesis
Keywords: piRNA, Piwi, TDRD12, Tudor, ECAT8
Classification: Biological Sciences (Developmental Biology)

[1]Equal contribution

[2]To whom correspondence may be addressed:
Ramesh S. Pillai
Phone: xx-33-4-76 20 7446
Fax: xx-33-4-76 20 7199
E-mail: pillai@embl.fr
Or
Shinya Yamanaka
Phone: +81-75-366-7044
Fax: +81-75-366-7024
E-mail: yamanaka@cira.kyoto-u.ac.jp

Author Contributions: R.R.P., Y.T., Z.Y., S.C., S.Y., and R.P. designed research; R.R.P., Y.T., Z.Y., T.I., E.H., S.K., Y.A. and T.K. performed research; R.S. analyzed data; and R.P wrote the paper.

\body

SUMMARY

Piwi-interacting RNAs (piRNAs) are gonad-specific small RNAs that provide defence against transposable genetic elements called transposons. Our knowledge of piRNA biogenesis is sketchy, partly due to an incomplete inventory of the factors involved. Here, we identify Tudor domain-containing 12 (TDRD12; also known as ECAT8) as a novel piRNA biogenesis factor in mice. TDRD12 is detected in complexes containing MILI (PIWIL2), its associated primary piRNAs, and TDRD1, all of which are already implicated in secondary piRNA biogenesis. Male mice carrying either a nonsense point mutation (*repro23* mice) or a targeted deletion in the *Tdrd12* locus are infertile, and de-repress retrotransposons. We find that TDRD12 is dispensable for primary piRNA biogenesis but essential for production of secondary piRNAs that enter MIWI2 (PIWIL4). Cell culture studies with the insect orthologue of TDRD12 suggest a role for the multi-domain protein in mediating complex formation with other participants during secondary piRNA biogenesis.

INTRODUCTION

Repetitive mobile genomic elements called transposons are a potential source of mutations causing genome instability. They are particularly active in the germline as mobilization can be inherited, allowing them to spread in the population. To counter this threat, animal germlines have evolved a dedicated class of 24-30 nucleotide (nt) long small RNAs called Piwi-interacting RNAs (piRNAs) (1-3). In mice, the piRNA pathway is mainly active in the male germline where all the three Piwi proteins (MILI, MIWI and MIWI2) are expressed. Nuclear MIWI2 is implicated in establishing transcriptional silencing in embryonic germ cells by deposition of DNA methylation marks on target transposon loci (4, 5). Cytoplasmic MILI and MIWI have a role in maintaining repression by direct cleavage of transposon transcripts using their endonucleolytic (Slicer) cleavage activity (6-8).

Biogenesis of piRNAs is only beginning to be understood, but two biochemically distinct pathways can be discerned. Primary biogenesis describes conversion of long, single-stranded transcripts arising from genomic loci called piRNA clusters (up to 100 kilobases long) into 24-30 nt piRNAs that associate with MILI and MIWI (9). On the other hand, biogenesis of MIWI2-bound piRNAs is indirect, whereby MILI-mediated slicer cleavage of a target is proposed to initiate production of a new secondary piRNA (4, 5, 7). This arrangement allows germ cells to monitor activity of transposons and adaptively respond to it by guiding MIWI2 to their genomic loci. Events that follow the initial MILI cleavage of a target are unknown, partly because of an incomplete knowledge of the components involved. Here, we identify TDRD12 in mouse Piwi complexes and demonstrate its *in vivo* role in secondary piRNA biogenesis and transposon silencing.

RESULTS

TDRD12 is a component of the MILI ribonucleoprotein complex

Piwi proteins are post-translationally modified at their N-termini by symmetrical dimethyl arginine (sDMA) marks which serve as ligands for tudor domains found in Tudor domain-containing (TDRD) proteins (10). Previous proteomic studies of mouse Piwi complexes have identified almost every member of the TDRD family (6, 11, 12). Uniquely, TDRD12 (also called ES-cell associated transcript 8, ECAT8) (13) was never detected. TDRD12 is composed of a central helicase and two flanking tudor domains, along with a C-terminal CS domain (as present in CHORD-SGT1 proteins) (Fig. 1A). It is highly conserved and represented by a single gene in insects to human. The *Drosophila* genome on the other hand has three members: Yb, Brother of Yb (BoYb) and Sister of Yb (SoYb), all of which are implicated in transposon control. Additionally, Yb is shown to be essential for primary piRNA biogenesis in the ovarian somatic follicle cells (14, 15). We wished to examine the involvement of TDRD12 in the mouse piRNA pathway.

Like most members of the TDRD family, *Tdrd12* expression is restricted to the mouse gonads, and its expression domain extends from embryonic to the adult stages in mouse testes (Fig. S1A). We examined its presence in purified MILI complexes isolated from adult testes (Fig. 1B). Consistent with previous Piwi proteomics data (11, 16), TDRD12 was not detected in the MILI immunoprecipitates, while TDRD1, an established interacting partner of MILI was present (Fig. 1B and S1B-C). Nevertheless, direct immunoprecipitation of TDRD12 identified MILI and TDRD1 as components, suggesting that only a sub-population of MILI is in complex with TDRD12, possibly explaining why it went undetected previously.

Interaction between MILI and TDRD1 is mediated via recognition of sDMA marks on MILI by the aromatic cage within tudor domains of TDRD1 (17). However, a sequence alignment of tudor domains from known sDMA-binders and those from TDRD12 orthologues reveals that amino acid residues critical for constructing such an aromatic cage are absent in the TDRD12 proteins (Fig. 1C). This predicted inability to recognize modified arginine was confirmed by isothermal calorimetry (ITC) measurements (Fig. S1D-E). Thus, direct interaction between MILI and TDRD12, if any, should be independent of the methylation status of MILI. Interestingly, RNase-treatment reduced the recovery of MILI in TDRD12 complexes, indicating the importance of RNA for complex formation (Fig. 1B and Fig. S1C). This prompted us to ask whether MILI-bound small RNAs are present in the complex. We prepared two independent deep sequencing libraries of small RNAs present in TDRD12 complexes from embryonic day 18.5 (E18.5) testes, where MILI and MIWI2 are co-expressed. The TDRD12 reads were found to have the same length profile (~26 nt) as MILI-bound piRNAs, but not that of the co-expressed MIWI2 (~28 nt) (Fig. 1D). Based on further analyses of nucleotide preferences (Fig. S2A), and mappings to transposon consensus and embryonic clusters (data not shown), the small RNAs in TDRD12 complexes can be identified as those that normally guide MILI in fetal germ cells. Presence of TDRD1 was not affected by the RNase-treatment (Fig. 1B), indicating its recruitment via protein-protein interactions with an unknown partner within the complex, as TDRD1 and TDRD12 did not interact directly (Fig. S2B). Taken together, TDRD12 exists in a

biochemical complex containing TDRD1 and the MILI piRNP, linking it to the mouse piRNA pathway.

Roles of Tdrd12 domains

To gain further insight into the function of TDRD12, we wished to examine the importance of its multiple domains *in vivo*. As mammalian cell culture models suitable for piRNA studies are unavailable, we used the *Bombyx mori* BmN4 insect cell culture system (18). BmN4 cells express two Piwi proteins, Siwi and Ago3, which display all known features of the piRNA pathway found in the *Drosophila* germline. Important for our study, Siwi binds primary piRNAs, while Ago3 accumulates secondary piRNAs, very much analogous to mouse Piwi proteins MILI and MIWI2, respectively.

We mined a polyA+ trascriptome library to identify *Bombyx mori* Tdrd12 (BmTdrd12) as the sole Tdrd12 representative in BmN4 cells (Fig. 2A and see Methods). Using specific antibodies to the endogenous BmTdrd12 (Fig. S3A), we demonstrate its presence in a complex with endogenous Siwi, but not Ago3 (Fig. 2B). This is further confirmed with tagged Piwi proteins (Fig. 2C). Deep sequencing of small RNAs in HA-BmTdrd12 and endogenous BmTdrd12 complexes supports the biochemical association data by identifying small RNAs that share sequence features (Fig. 2D), and transposon-mapping characteristics that are similar to Siwi-bound piRNAs (Fig. S3B). Thus, similar to mouse TDRD12, the *Bombyx* orthologue is also in complex with the primary piRNA-bound Piwi protein (MILI in mouse testes or Siwi in BmN4), validating BmN4 cells as a useful system for molecular dissections. Using deletion versions (Fig. 2A), we map the interaction domain for Siwi to the 2nd tudor domain of HA-BmTdrd12 (Fig. 2E).

Piwi proteins display distinct localization patterns in BmN4 cells. Siwi is distributed throughout the cytoplasm, whereas Ago3 is sequestered in perinuclear cytoplasmic granules called nuage (19). Unexpectedly, although HA-BmTdrd12 interacts with Siwi, it is found co-localized with Ago3 in the nuage (Fig. 2F). Deletion of the CS domain (construct A) abolished this localization (Fig. 2F). All other deletion constructs (constructs B and C) were also found to be diffused in the cytoplasm (data not shown). Next, to examine the importance of the helicase domain, we introduced mutations (20) to perturb ATP-binding (K→A) or hydrolysis (DD→AA). Mutation of the ATPase motif resulted in a substantial displacement of the protein from the nuage, while mutation of the ATP-binding motif did not (Fig. 2F). Importantly, all helicase point mutants (Fig. 2G) and the deletion version lacking the CS domain (Fig. 2E) showed interaction with Siwi, indicating that their association can occur in the cytoplasm prior to nuage-localization. In sum, these cell culture experiments reveal contributions of BmTdrd12 domains to interaction with the Piwi protein and nuage localization.

***Tdrd12* is essential for spermatogenesis**

To examine the *in vivo* role of TDRD12, we first examined the *repro23* point mutant which was generated by *N*-ethyl-*N*-nitrosourea (ENU)-induced mutagenesis. The *repro 23* mutation was previously mapped to a region containing several genes, including *Tdrd12* (21). In this study, we identify it as a nonsense mutation in exon 8 of the *Tdrd12* gene, truncating the coding sequence (Fig.

3A). Since homozygous *repro23* mutant mice display male infertility (21), this suggests a potential role for TDRD12 in mouse spermatogenesis. To directly verify this, we engineered a targeted disruption of the mouse *Tdrd12* locus (Fig. S4A-C). Animals of all genotypes are viable and females are fertile, but homozygous *Tdrd12* mutant males displayed infertility and had atrophied testes (Fig. 3B). Histological examination of *Tdrd12* mutant testes reveals seminiferous tubules that are narrow with large vacuolated spaces, devoid of late-stage germ cells. In contrast, the testes from heterozygous littermates contain germ cells of all developmental stages: meiotic spermatocytes, post-meiotic round spermatids and elongating spermatids (Fig. 3C). The germ cell defect in the mutant is apparent early in development and spermatocytes fail to proceed beyond the pre-pachytene stage (Fig. S4D). The XY body, a γ-H2AX-marked silent chromatin domain containing unpaired X and Y chromosomes in late zygotene to pachytene spermatocytes, is absent in the mutant (Fig. S4E). Finally, post-meiotic round spermatids and their gene products are also not detected (Fig. S4F). Thus, germ cell development falters during meiosis in the zygotene-pachytene transition and the cells go into apoptosis, as indicated by the high number of TUNEL-positive cells in P20 and adult mutant testes (Fig. S4G). These results illustrate an essential role of *Tdrd12* for normal spermatogenesis, a hallmark of all mouse piRNA pathway mutants.

Retrotransposons are derepressed in the *Tdrd12* mutants

The germ cell defect in piRNA pathway mutants is believed to be a consequence of deregulated transposon control in the germline. Consistently, derepression of LTR IAP elements is already observed in 10-day old (P10) mutant animals (Fig. 3D), at a time point when the germ cell defects are not histologically discernible (Fig. S4D). Non-LTR LINE1 (L1) activation was delayed, with robust levels of L1 mRNA detected only in P24 testes, but the levels of both transposons remain high in aged (P60 and P100) animals (Fig. 3D). L1 activation was further confirmed in adult mutants by immunofluorescence detection of L1ORF1p (22), a protein product from active L1 elements (Fig. 3E). Furthermore, we also confirm derepression of retrotransposons in the *repro23* point mutant (Fig. S4H).

Mammalian genomes employ DNA methylation as a mechanism to silence transposons at the level of transcription (23). In male mice, this takes place during a developmental window immediately prior to birth, when DNA methylation marks are laid down *de novo*. We examined the DNA methylation status by bisulfite sequencing using genomic DNA from purified spermatogonia. In *Tdrd12* mutants, promoter methylation on CpG dinucleotides was reduced for both L1 (53%) and IAP (61%) elements when compared to their heterozygous littermates (~90%), suggesting a defect in their *de novo* methylation (Fig. 3F). Although repeat elements are the major beneficiaries of *de novo* DNA methylation, imprinted genomic loci also receive silencing marks during this period. Examination of methylation on three imprinted loci in *Tdrd12* mutants revealed no changes (Fig. S5A), underscoring the specificity of the piRNA pathway in targeting repeat elements in the fetal male germline. Thus, TDRD12 is essential for germ cells in maintaining control over endogenous retrotransposons.

TDRD12 is required for biogenesis of MIWI2 piRNAs

Deposition of DNA methylation marks on repeat elements is linked to the nuclear arm of the piRNA pathway, a key player of which is the nuclear Piwi protein MIWI2. Functionality of MIWI2 is dependent on production and incorporation of its small RNA guides via secondary processing (4). To examine the integrity of piRNA biogenesis, we purified total small RNAs (14-40 nt) from P0 (new-born) testes and subjected them to deep sequencing. As expected for mouse testes small RNA libraries, the read-length distribution profiles reveal two major peaks expected for miRNAs (19-22 nt) and piRNAs (24-30 nt) in both the *Tdrd12* mutant and heterozygous littermates, with overall level of piRNAs slightly reduced in the mutant (Fig. 4A). Examined over IAP consensus sequence, much of this reduction is accounted for by antisense-oriented reads (Fig. 4B). This is further strengthened by the observation that ratio of antisense to sense piRNAs over both LINE1 and IAP was reduced in the *Tdrd12* mutant (Fig. 4C). Since MILI- and MIWI2-bound RNAs contribute to total small RNA populations in P0 testes, we directly determined the impact on these individual populations by immunoprecipitations. In the control testes, both MILI and MIWI2 are present in complex with distinctly-sized small RNAs (Fig. 4D). In contrast, only MILI was found to associate with piRNAs in the *Tdrd12* mutant (three independent experiments), suggesting a defect in biogenesis of piRNAs that normally associate with MIWI2 (Fig. 4D and Fig. S5B). Since loading of MIWI2 with piRNAs is a prerequisite for its nuclear import, unloaded MIWI2 remains stranded in the cytoplasm of E17.5 germ cells (gonocytes) in the *Tdrd12* mutant (Fig. 4E).

Primary piRNAs associating with MILI are proposed to guide its slicer activity for biogenesis of MIWI2 piRNAs (4, 7). An outcome of this pathway is the detected 10 nt overlap between 5' ends of MILI- and MIWI2-bound piRNAs (4). A similar signature is also evident in total small RNA populations from the *Tdrd12* hetrozygous animals, but consistent with the loss of MIWI2-bound piRNAs, is absent in the *Tdrd12* mutants (Fig. 4F). As shown above, biogenesis of piRNAs associating with Mili appeared normal in the lack of *Tdrd12* (Fig. 4D). To examine this at the molecular level, two independent libraries of MILI-bound piRNAs were prepared from *Tdrd12* mutant or control P0 animals, and subjected to deep sequencing. Analysis indicates unchanged genome annotation profiles (Fig. S5C) and signature 1U-bias of primary piRNAs in the mutant (Fig. S5D). The distribution on transposon consensus sequences and piRNA clusters are also not affected (Fig. S5E-F). Furthermore, immunoprecipitations confirm that primary biogenesis continues to supply piRNAs for MILI in postnatal (P10 and P14) *Tdrd12* mutants (Fig. S5G). These analyses indicate that primary piRNA-loaded MILI remains competent to initiate secondary biogenesis, but in the absence of TDRD12, downstream events fail.

Factors implicated in piRNA biogenesis occupy distinct cytoplasmic granules in germ cells called nuages. In mouse fetal germ cells, they appear as electron-dense structures between mitochondria, the so-called intermitochondrial cement (24, 25). Our repeated efforts to localize TDRD12 failed, possibly due to the unsuitability of our antibodies for immunofluorescence or due to the low abundance of the protein. Nevertheless, we show that sub-cellular localization of MILI and

TDRD1 are not affected in the *Tdrd12* mutant (Fig. 4E and Fig. S4I). Furthermore, electron micrographs also reveal the normal presence of the intermitochondrial cement (in three biological replicates), suggesting the absence of any defect in granule assemblies in the mutant germ cells (Fig. S5H). In the light of the above data, we propose a direct role for TDRD12 in the machinery that generates the secondary piRNAs associating with MIWI2.

DISCUSSION

Biogenesis of piRNAs is only beginning to be understood and progress has to be made on two fronts: identification of the complete set of factors involved and molecular mechanisms employed by them. Here we identified TDRD12 as a new mouse piRNA biogenesis factor. The ability to produce piRNAs rests with a few hundred genomic regions called piRNA clusters, some of which are up to 100 kilobases in length. These are transcribed by RNA polymerase II to give rise to long, single-stranded transcripts that are 5' capped and polyadenylated, with some undergoing splicing too (9). At least for a subset of these clusters (those producing intergenic piRNAs), the transcription factor A-MYB is shown to directly recognize upstream DNA elements to initiate transcription (9) (Fig. 4G). The transcripts are then exported to the cytoplasm where they undergo primary processing which is likely to include fragmentation by unknown nuclease(s) followed by loading of their 5' ends into the Piwi proteins (MILI or MIWI). The protruding 3' ends of such piRNA intermediates are then trimmed by an exonuclease (tentatively termed as Trimmer)(26) to the mature size as determined by the footprint of the Piwi protein. Finally, the 3' end is modified by the 2'-O-methyltransferase HEN1 to complete the process, resulting in primary piRNAs with a predominant preference for a 5' uridine (1U-bias). Currently, the putative RNA helicase MOV10L1 (27, 28) and the single-stranded endonuclease MitoPLD (29-31) are implicated in the early steps, but the exact substrates and products of these factors are not known. TDRD2 (32) is shown to be essential for recruitment of the Trimmer, as piRNAs with extended 3' ends (and properly methylated) accumulate in MILI in *Tdrd2* mutant mice. GASZ (33) is a structural component of perinuclear cytoplasmic granules variably called nuage or intermitochondrial cement where most piRNA pathway factors accumulate. Loss of *Gasz* results in reduced piRNA levels and destabilization of the (unloaded) MILI. Primary piRNA-loaded MILI and MIWI slice target transcripts to ensure transposon silencing.

In fetal mouse germ cells, primary piRNA-guided MILI endonuclease action on a target is proposed to create the 5' end of new secondary piRNA entering MIWI2 (4, 7). Piwi slicer activity is mechanistically similar to that mediated by Ago proteins in the RNA-induced silencing complex (RISC) (6, 34). However, unlike in the RISC where both fragments are degraded, one of the MILI-generated cleavage fragments is believed to mature as a new secondary piRNA (4, 7). How the cleavage fragment is safely transferred to MIWI2 is not known. Additional factors that are essential for secondary biogenesis include the RNA helicase MVH (35), Hsp90 co-chaperone Fkbp6 (19) and TDRD1 (11, 16). It is possible that RNA helicases like MVH and TDRD12 might facilitate RNP remodelling required for inter-Piwi exchange of piRNA intermediates.

Our biochemical studies indicate that TDRD12 functions together with other secondary biogenesis factors like the MILI piRNP and TDRD1 (Fig. 1). Nevertheless, we cannot rule out the presence of unloaded MIWI2 within this complex. Within this complex, the tudor domains of TDRD12 are likely to engage MILI in a methylation-independent manner (Fig. 1C). Although a direct comparison of the mouse and *Bombyx* systems is not possible, the 2nd tudor domain of mouse TDRD12 could be mediating the interaction with MILI. Furthermore, sensitivity of MILI-TDRD12 association to RNase-treatment (Fig. 1B) raises the possibility that RNAs present in the complex could be targets of MILI-bound primary piRNAs, and hence substrates for secondary biogenesis. Finally, our studies with the insect orthologue of mouse TDRD12 revealed a role for the CS domain in nuage localization. The CS domain is a reported protein-protein interaction domain, which some co-chaperones use to recruit the molecular chaperones HSP90 and HSP70 (36, 37). We explored this exprimentally, but ourexperiments do not support such a role for the CS domain from TDRD12 (Fig. S2C-D).It is possible that interaction with unknown nuage components might allow its retention in the granules. Future live cell imaging and structural studies will be important in uncovering the exact molecular function of this multi-domain protein in piRNA biogenesis.

EXPERIMENTAL PROCEDURES

Detailed information on materials and methods is provided in online Supporting Information. All Illumina deep sequencing data described in this paper are deposited with Gene Expression Omnibus (GEO) (GSEXXXX). The *TDRD12* mutant mouse is available from the RIKEN Bio resource center (Acc. No. RBRC02326).

FIGURE LEGENDS

Fig. 1. TDRD12 associates with mouse secondary piRNA biogenesis factors

(A) Domain organization of TDRD12 proteins in mouse (Mm), *Drosophila* (Dm) and *Bombyx* (Bm). (B) Immunoprecipitated (IP) complexes were probed by Western analysis for the indicated proteins. +RNaseA, treatment with RNaseA. (C) Sequence alignment of tudor domain from proteins demonstrated to bind symmetrical dimethyl arginine (sDMA), and those from TDRD12 proteins. Aromatic cage residues essential for binding sDMA are highlighted in red. (D) The read-length distribution in small RNA libraries from indicated proteins.

Fig. 2. Roles of Tdrd12 domains in Piwi interaction and nuage localization

(A) Domain organization of *Bombyx* Tdrd12 (BmTdrd12). An HA-tagged version lacking the N-terminal region (259 aa) was used for cell culture studies (see Methods). Other deletion versions used in this study are indicated (B) Immunoprecipitated (IP) endogenous BmTdrd12 associates with endogenous Piwi protein Siwi. (C) HA-tagged Siwi, but not HA-Ago3, associates with endogenous BmTdrd12. (D) The nucleotide bias for a uridine at 1st position (1U) or adenosine at 10th position

(A10) of reads in small RNA libraries is shown. (E) Analysis of HA-BmTdrd12 deletion versions for association with endogenous Siwi. (F) Sub-cellular localization of HA-BmTdrd12 and its mutants. Alignment of helicase domains from indicated proteins showing critical residues required for ATP-binding or hydrolysis. Residues mutated in HA-BmTdrd12 are highlighted in red. (G) Helicase domain mutations in HA-BmTdrd12 do not affect association with endogenous Siwi.

Fig. 3. *Tdrd12* mutant male mice are infertile and display de-repression of retrotransposons

(A) The nonsense C-to-A nucleotide substitution in exon 8 of *Tdrd12* in *repro23* mice leads to truncation of the coding sequence. (B) Atrophied testes of homozygous (-/-) *Tdrd12* mutants compared to their heterozygous (+/-) littermates. (C) Hematoxylin and eosin staining of adult testes sections from *Tdrd12* animals. sp, spermatocytes; rs, round spermatids; es, elongating spermatids. Scale =20 μm. (D) Northern analysis for LINE1 (L1) and IAP retrotransposons in *Tdrd12* mutants. Only L1 elements are activated in *Tdrd1* mutants. Loading control is provided by ethidium bromide staining of ribosomal RNA (rRNA). (E) Immunofluorescence detection of L1ORF1p in adult *Tdrd12* mutant testis. (F) Promoter CpG DNA methylation (indicated as filled circles) on transposon promoters quantified (in percentages) by bisulfite sequencing.

Fig. 4. TDRD12 is required for biogenesis of MIWI2-bound secondary piRNAs

(A) Read-length distribution profile of testes total small RNAs from indicated animals. (B) Normalized (to microRNAs) density of reads mapping to IAP transposon consensus from P0 total small RNA libraries. Note the reduction of antisense reads in the *Tdrd12* mutant. (C) Ratio of antisense/sense piRNAs mapping LINE1 or IAP consensus. (D) Association of piRNAs with Piwi proteins examined by immunoprecipitation and 5'-end labelling from new born pups (P0). RNA markers (nucleotides, nt) are shown. (E) Immunofluorescence detection of proteins in embryonic testes from indicated *Tdrd12* genotypes. Images (green) are shown along with DAPI staining for DNA. Scale =10 μm. Note the loss of nuclear MIWI2 staining in *Tdrd12* mutants. (F) Plot showing 5'-end overlap of opposing reads on IAP consensus in total small RNA libraries. Note the reduction in signal at position 10 (Ping-Pong signature) in the *Tdrd12* mutant. (G) Current knowledge on factors implicated in the mouse piRNA pathway, and placement of TDRD12 as a secondary piRNA biogenesis factor.

ACKNOWLEDGMENTS

We acknowledge the kind gift of antibody from Sandra Martin (L1ORF1p). We thank Anna Adamiok, Charlotta Funaya, Andres Palencia and Nikos Mathioudakis for assistance with experiments, and Jafar Sharif and Kohzoh Mitsuya for bisulfite data. T.K is funded by Japan Society for the Promotion of Science (JSPS). S.C. is grateful to Norio Nakatsuji and supported by grants-in-aid for scientific research, MEXT, Japan. R.R.P is supported by EMBL Interdisciplinary Postdoctoral (EIPOD) and EMBO Long Term Fellowships. This work was funded by a European Research Council Starting

Grant (pisilence) from the European Union to R.S.P. The R.S.P. laboratory is supported by the EMBL.

REFERENCES

1. Malone CD & Hannon GJ (2009) Small RNAs as guardians of the genome. *Cell* 136(4):656-668.
2. Ghildiyal M & Zamore PD (2009) Small silencing RNAs: an expanding universe. *Nat Rev Genet* 10(2):94-108.
3. Siomi MC, Sato K, Pezic D, & Aravin AA (2011) PIWI-interacting small RNAs: the vanguard of genome defence. *Nat Rev Mol Cell Biol* 12(4):246-258.
4. Aravin AA*, et al.* (2008) A piRNA pathway primed by individual transposons is linked to de novo DNA methylation in mice. *Mol Cell* 31(6):785-799.
5. Kuramochi-Miyagawa S*, et al.* (2008) DNA methylation of retrotransposon genes is regulated by Piwi family members MILI and MIWI2 in murine fetal testes. *Genes Dev* 22(7):908-917.
6. Reuter M*, et al.* (2011) Miwi catalysis is required for piRNA amplification-independent LINE1 transposon silencing. *Nature* 10.1038/nature10672.
7. De Fazio S*, et al.* (2011) The endonuclease activity of Mili fuels piRNA amplification that silences LINE1 elements. *Nature*.
8. Di Giacomo M*, et al.* (2013) Multiple epigenetic mechanisms and the piRNA pathway enforce LINE1 silencing during adult spermatogenesis. *Mol Cell* 50(4):601-608.
9. Li XZ*, et al.* (2013) An ancient transcription factor initiates the burst of piRNA production during early meiosis in mouse testes. *Mol Cell* 50(1):67-81.
10. Siomi MC, Mannen T, & Siomi H (2010) How does the royal family of Tudor rule the PIWI-interacting RNA pathway? *Genes Dev* 24(7):636-646.
11. Vagin VV*, et al.* (2009) Proteomic analysis of murine Piwi proteins reveals a role for arginine methylation in specifying interaction with Tudor family members. *Genes Dev*.
12. Chen C*, et al.* (2009) Mouse Piwi interactome identifies binding mechanism of Tdrkh Tudor domain to arginine methylated Miwi. *Proc Natl Acad Sci U S A*.
13. Mitsui K*, et al.* (2003) The homeoprotein Nanog is required for maintenance of pluripotency in mouse epiblast and ES cells. *Cell* 113(5):631-642.
14. Handler D*, et al.* (2011) A systematic analysis of Drosophila TUDOR domain-containing proteins identifies Vreteno and the Tdrd12 family as essential primary piRNA pathway factors. *Embo J* 30(19):3977-3993.
15. Saito K*, et al.* (2010) Roles for the Yb body components Armitage and Yb in primary piRNA biogenesis in Drosophila. *Genes Dev* 24(22):2493-2498.
16. Reuter M*, et al.* (2009) Loss of the Mili-interacting Tudor domain-containing protein-1 activates transposons and alters the Mili-associated small RNA profile. *Nat Struct Mol Biol* 16(6):639-646.
17. Mathioudakis N*, et al.* (2012) The multiple Tudor domain-containing protein TDRD1 is a molecular scaffold for mouse Piwi proteins and piRNA biogenesis factors. *Rna* 18(11):2056-2072.
18. Kawaoka S*, et al.* (2009) The Bombyx ovary-derived cell line endogenously expresses PIWI/PIWI-interacting RNA complexes. *Rna* 15(7):1258-1264.
19. Xiol J*, et al.* (2012) A Role for Fkbp6 and the Chaperone Machinery in piRNA Amplification and Transposon Silencing. *Mol Cell* 47(6):970-979.
20. Linder P & Jankowsky E (2011) From unwinding to clamping - the DEAD box RNA helicase family. *Nat Rev Mol Cell Biol* 12(8):505-516.
21. Asano Y*, et al.* (2009) Characterization and linkage mapping of an ENU-induced mutant mouse with defective spermatogenesis. *Exp Anim* 58(5):525-532.
22. Branciforte D & Martin SL (1994) Developmental and cell type specificity of LINE-1 expression in mouse testis: implications for transposition. *Mol Cell Biol* 14(4):2584-2592.

23. Reik W (2007) Stability and flexibility of epigenetic gene regulation in mammalian development. *Nature* 447(7143):425-432.
24. Aravin AA*, et al.* (2009) Cytoplasmic compartmentalization of the fetal piRNA pathway in mice. *PLoS Genet* 5(12):e1000764.
25. Chuma S, Hosokawa M, Tanaka T, & Nakatsuji N (2009) Ultrastructural characterization of spermatogenesis and its evolutionary conservation in the germline: germinal granules in mammals. *Mol Cell Endocrinol* 306(1-2):17-23.
26. Kawaoka S, Izumi N, Katsuma S, & Tomari Y (2011) 3' end formation of PIWI-interacting RNAs in vitro. *Mol Cell* 43(6):1015-1022.
27. Zheng K*, et al.* (2010) Mouse MOV10L1 associates with Piwi proteins and is an essential component of the Piwi-interacting RNA (piRNA) pathway. *Proc Natl Acad Sci U S A* 107(26):11841-11846.
28. Frost RJ*, et al.* (2010) MOV10L1 is necessary for protection of spermatocytes against retrotransposons by Piwi-interacting RNAs. *Proc Natl Acad Sci U S A* 107(26):11847-11852.
29. Watanabe T*, et al.* (2011) MITOPLD is a mitochondrial protein essential for nuage formation and piRNA biogenesis in the mouse germline. *Dev Cell* 20(3):364-375.
30. Ipsaro JJ, Haase AD, Knott SR, Joshua-Tor L, & Hannon GJ (2012) The structural biochemistry of Zucchini implicates it as a nuclease in piRNA biogenesis. *Nature* 491(7423):279-283.
31. Nishimasu H*, et al.* (2012) Structure and function of Zucchini endoribonuclease in piRNA biogenesis. *Nature* 491(7423):284-287.
32. Saxe JP, Chen M, Zhao H, & Lin H (2013) Tdrkh is essential for spermatogenesis and participates in primary piRNA biogenesis in the germline. *Embo J* 32(13):1869-1885.
33. Ma L*, et al.* (2009) GASZ is essential for male meiosis and suppression of retrotransposon expression in the male germline. *PLoS Genet* 5(9):e1000635.
34. Meister G & Tuschl T (2004) Mechanisms of gene silencing by double-stranded RNA. *Nature* 431(7006):343-349.
35. Kuramochi-Miyagawa S*, et al.* (2010) MVH in piRNA processing and gene silencing of retrotransposons. *Genes Dev* 24(9):887-892.
36. Buchner J, Weikl T, Bugl H, Pirkl F, & Bose S (1998) Purification of Hsp90 partner proteins Hop/p60, p23, and FKBP52. *Methods Enzymol* 290:418-429.
37. Takahashi A, Casais C, Ichimura K, & Shirasu K (2003) HSP90 interacts with RAR1 and SGT1 and is essential for RPS2-mediated disease resistance in Arabidopsis. *Proc Natl Acad Sci U S A* 100(20):11777-11782.

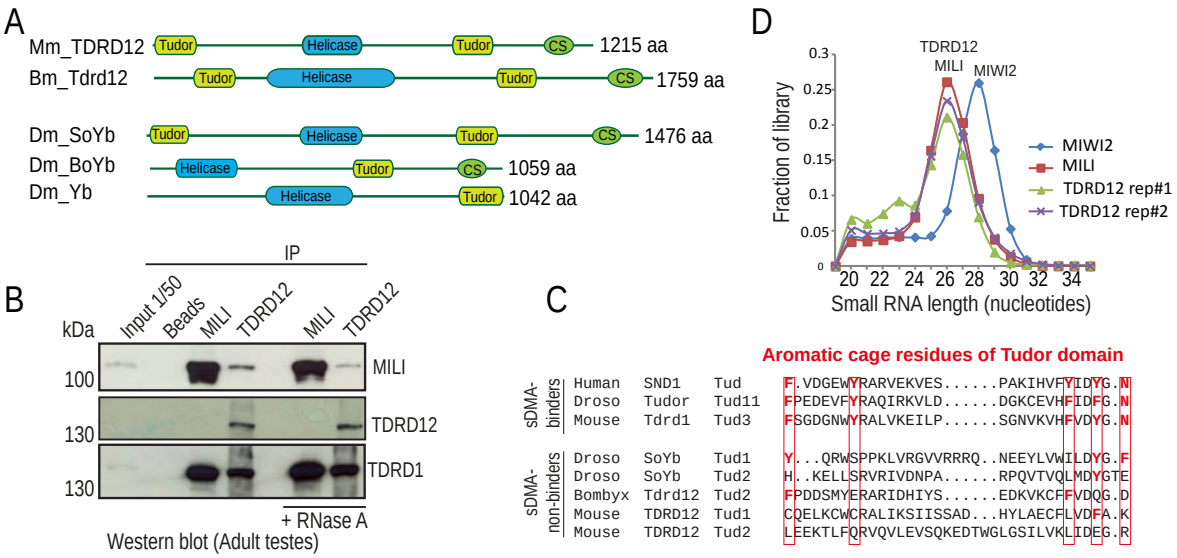
A
Mm_TDRD12
Tudor
Helicase
Tudor
CS
1215 aa
Bm_Tdrd12
1759 aa
Dm_SoYb
1476 aa
Dm_BoYb
1059 aa
Dm_Yb
1042 aa
B
IP
kDa
Input 1/50
Beads
MILI
TDRD12
MILI
TDRD12
100
MILI
130
TDRD12
130
TDRD1
+ RNase A
Western blot (Adult testes)
C
Aromatic cage residues of Tudor domain
sDMA-binders
Human SND1 Tud F.VDGEWYRARVEKVES.....PAKIHVFYIDYG.N
Droso Tudor Tud11 FPEDEVFYRAQIRKVLD.....DGKCEVHFIDFG.N
Mouse Tdrd1 Tud3 FSGDGNWYRALVKEILP.....SGNVKVHFVDYG.N
sDMA-non-binders
Droso SoYb Tud1 Y...QRWSPPKLVRGVVRRRQ..NEEYLVWILDYG.F
Droso SoYb Tud2 H..KELLSRVRIVDNPA.....RPQVTVQLMDYGTE
Bombyx Tdrd12 Tud2 FPDDSMYERARIDHIYS.....EDKVKCFFVDQG.D
Mouse TDRD12 Tud1 CQELKCWCRALIKSIISSAD...HYLAECFLVDFA.K
Mouse TDRD12 Tud2 LEEKTLFQRVQVLEVSQKEDTWGLGSILVKLIDEG.R
D
TDRD12
MILI
MIWI2
Fraction of library
0.3
0.25
0.2
0.15
0.1
0.05
0
20 22 24 26 28 30 32 34
Small RNA length (nucleotides)
MIWI2
MILI
TDRD12 rep#1
TDRD12 rep#2

Fig. 1

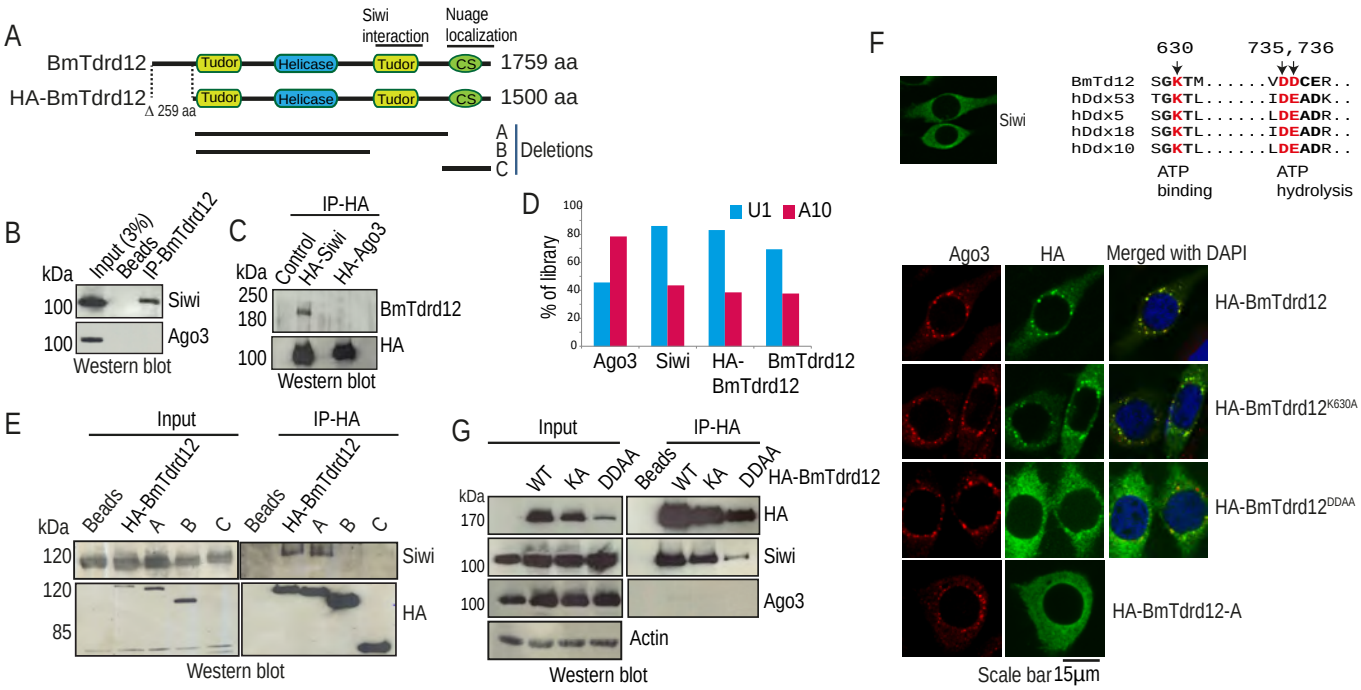
A
Siwi interaction
Nuage localization
BmTdrd12
Tudor
Helicase
Tudor
CS
1759 aa
HA-BmTdrd12
Δ 259 aa
Tudor
Helicase
Tudor
CS
1500 aa
A
B
C
Deletions
B
kDa
Input (3%)
Beads
IP-BmTdrd12
100
Siwi
100
Ago3
Western blot
C
IP-HA
kDa
Control
HA-Siwi
HA-Ago3
250
180
BmTdrd12
100
HA
Western blot
D
U1
A10
% of library
100
80
60
40
20
0
Ago3
Siwi
HA-BmTdrd12
BmTdrd12
E
Input
IP-HA
kDa
Beads
HA-BmTdrd12
A
B
C
Beads
HA-BmTdrd12
A
B
C
120
Siwi
120
85
HA
Western blot
G
Input
IP-HA
WT
KA
DDAA
Beads
WT
KA
DDAA
HA-BmTdrd12
kDa
170
HA
100
Siwi
100
Ago3
Actin
Western blot
F
Siwi
630
735,736
BmTd12 SGKTM.....VDDCER..
hDdx53 TGKTL.....IDEADK..
hDdx5 SGKTL.....LDEADR..
hDdx18 SGKTL.....IDEADR..
hDdx10 SGKTL.....LDEADR..
ATP binding
ATP hydrolysis
Ago3
HA
Merged with DAPI
HA-BmTdrd12
HA-BmTdrd12K630A
HA-BmTdrd12DDAA
HA-BmTdrd12-A
Scale bar 15μm

Fig. 2

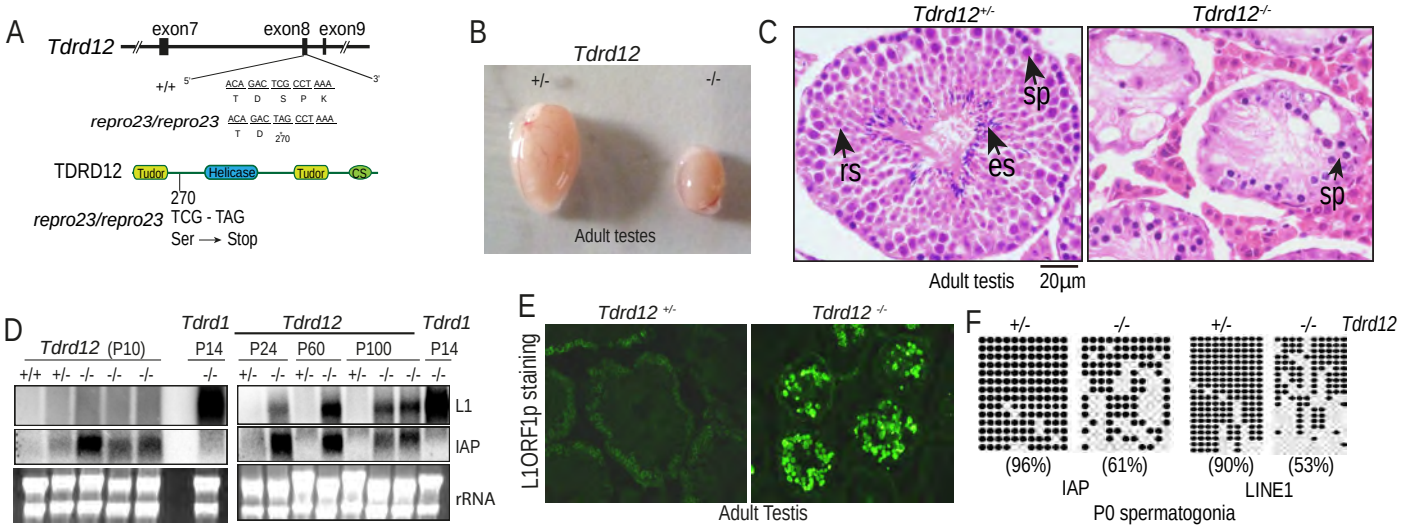
A
Tdrd12
exon7
exon8
exon9
+/+
ACA GAC TCG CCT AAA
T D S P K
repro23/repro23
ACA GAC TAG CCT AAA
T D
270
TDRD12
Tudor
Helicase
Tudor
CS
270
repro23/repro23
TCG - TAG
Ser → Stop
B
Tdrd12
+/-
-/-
Adult testes
C
Tdrd12+/-
Tdrd12-/-
sp
rs
es
sp
Adult testis
20µm
D
Tdrd12 (P10)
Tdrd1
Tdrd12
Tdrd1
P14
P24
P60
P100
P14
+/+ +/- -/- -/- -/-
-/-
+/- -/- +/- -/- +/- -/- -/- -/-
L1
IAP
rRNA
E
Tdrd12 +/-
Tdrd12 -/-
L1ORF1p staining
Adult Testis
F
+/-
-/-
+/-
-/-
Tdrd12
(96%)
(61%)
(90%)
(53%)
IAP
LINE1
P0 spermatogonia

Fig. 3

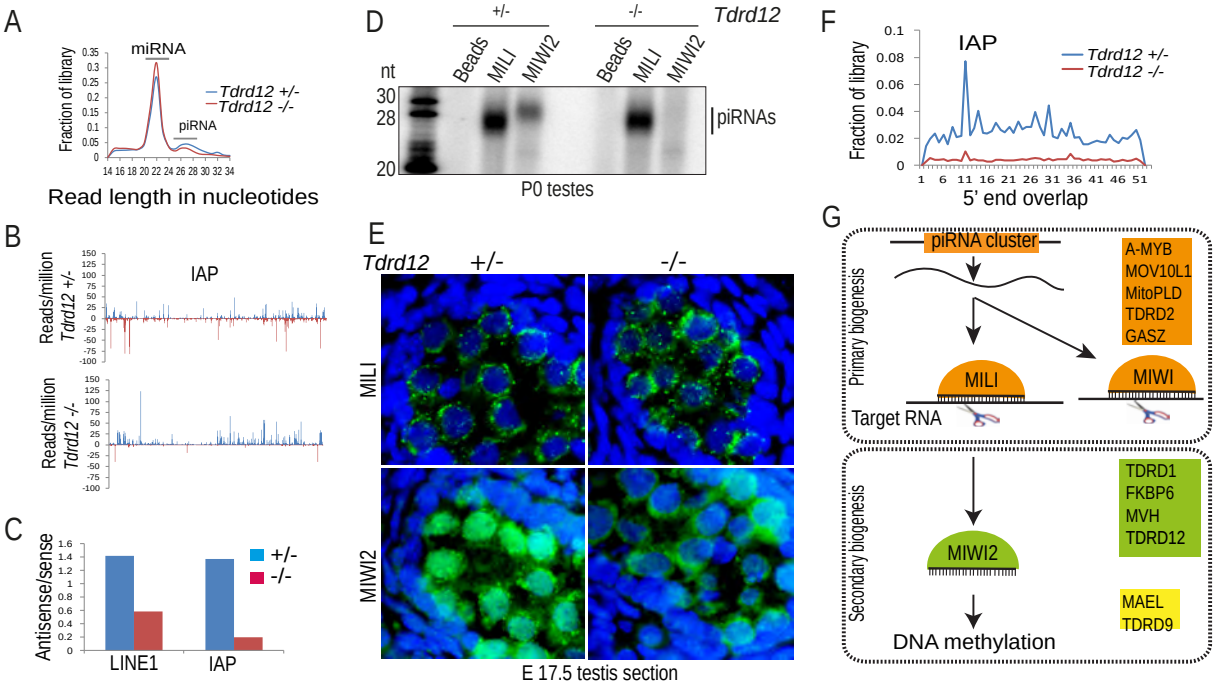
A
miRNA
piRNA
Tdrd12 +/-
Tdrd12 -/-
Fraction of library
Read length in nucleotides
B
IAP
Reads/million
Tdrd12 +/-
Tdrd12 -/-
C
Antisense/sense
+/-
-/-
LINE1
IAP
D
+/-
-/-
Tdrd12
Beads
MILI
MIWI2
nt
30
28
20
piRNAs
P0 testes
E
Tdrd12
+/-
-/-
MILI
MIWI2
E 17.5 testis section
F
IAP
Tdrd12 +/-
Tdrd12 -/-
Fraction of library
5' end overlap
G
piRNA cluster
A-MYB
MOV10L1
MitoPLD
TDRD2
GASZ
Primary biogenesis
MILI
MIWI
Target RNA
TDRD1
FKBP6
MVH
TDRD12
Secondary biogenesis
MIWI2
MAEL
TDRD9
DNA methylation

Fig. 4

Supporting information

Tudor domain containing 12 (TDRD12) is essential for secondary piRNA biogenesis in mice

Radha Raman Pandey, Yoshimi Tokuzawa, Zhaolin Yang, Eri Hayashi, Tomoko Ichisaka, Shimpei Kajita, Yuka Asano, Tetsuo Kunieda, Ravi Sachidanandam, Shinichiro Chuma, Shinya Yamanaka and Ramesh S. Pillai

SUPPORTING FIGURES AND LEGENDS

Fig. S1. *Tdrd12* expression in mouse tissues and its characterization

(A) RT-PCR expression analysis of *Tdrd12* expression in indicated adult mouse tissues or embryonic stem (ES) cells (top panel). The bottom panel shows RT-PCR expression analysis of *Tdrd12* expression in embryonic and adult mouse testes using primer pairs at N-terminal (Tdrd12-N term) and C-terminal (Tdrd12-C term) regions of *Tdrd12* coding region. (B) A cartoon depicting the domain organization of mouse TDRD12. The region used as an antigen for raising rabbit polyclonal antibodies is indicated. To test the specificity of the purified anti-TDRD12 antibodies, blots containing various proteins (HA- or Myc-tagged) expressed in HEK293T cells were probed with anti-TDRD12 antibodies. Only HA-TDRD12 was recognized by the antibodies, confirming its specificity. (C) Protein complexes were immunoprecipitated (IP) from adult mouse testes extracts and probed by Western analysis for the indicated proteins. When indicated, purified complexes were treated with RNaseA. This is a repetition of the experiment shown in Fig. 1B. (D) Coomassie blue stained SDS PAGE gel for the purified 2nd tudor domain (Tud2) of mouse TDRD12 expressed in *E.coli*. (E) Isothermal calorimetry (ITC) measurements of indicated TDRD1 or TDRD12 tudor domains with unmodified and methylated arginine residues. No interaction was detected with Tud2 of TDRD12, while the positive control (Tud3 of TDRD1) shows high micromolar-range affinity for sDMA (me2sym), as previously reported.

Fig. S2. Characterisation of mouse TDRD12 (A) The nucleotide bias for a uridine at 1st position (1U) or adenosine at 10th position (A10) of reads in the libraries is given. (B) HA- and Myc-tagged constructs were co-transfected in HEK293 cells and immunoprecipitated with HA affinity beads and probed for the co-immunoprecipitated Myc-tagged protein. As expected, TDRD1 interacts with MILI, while TDRD12 did not show an association with TDRD1. Human AGO2 (hAGO2) was used as negative control. (C) HA- and Myc-tagged constructs were co-transfected in HEK293T cell. Protein complexes were immunoprecipitated with HA-affinity beads and probed for co-imunoprecipitated Myc-tagged HSPA2 (HSP70) or endogenous HSP90 proteins. HSPA2 nonspecifically interacts with both mouse TDRD12 and hAGO2, while HSP90 does not interact with either full length mouse TDRD12 or its deletion variants. The CS domain in other proteins is shown to associate with the

molecular chaperones HSP70 and HSP90 (Buchner et al., 1998; Lee et al., 2004). But our experiments do not support such a role for the domain in TDRD12. (D) Coomassie-stained SDS-PAGE of purified GST-tagged CS domain of mouse TDRD12 expressed in BL21 *E.coli* cells (left panel). Pull-down experiment conducted with adult mouse testes extracts using GST alone or GST-CS peptide (right panel). None of the associated bands were revealed to be HSP90 or HSP70, as determined by MS/MS.

Fig. S3 Characterization of *Bombyx mori* Tdrd12

(A) Domain organization of predicted *Bombyx mori* Tdrd12 (BmTdrd12). The cDNA for BmTdrd12 corresponds to a protein encoding 1759 aa. In this study, an HA-tagged version of BmTdrd12 that lacks the N-terminal 259 aa was used, as we failed to express the tagged full length construct. Western blot analysis with purified BmTdrd12 antibodies detects a band of expected size (~200 kDa, expected from 1759 aa) in BmN4 cell lysates (left panel). The antibodies also recognize HA-BmTdrd12 expressed in BmN4 cells as an additional faster-migrating band (right panel). (B) Sequence analysis of the strand-orientation of piRNA reads in small RNA libraries prepared from HA-tagged BmTdrd12, endogenous BmTdrd12, HA-Siwi and HA-Ago3 complexes on indicated *Bombyx mori* transposon consensus sequences. The strand-orientation of reads from the BmTdrd12 and Siwi libraries are the same.

Fig. S4. Generation of the targeted *Tdrd12* mutant

(A) Schematic showing the targeted disruption of the mouse *Tdrd12* locus in RF8 ES cells. By homologous recombination, the targeting vector replaced exon 3 and 4 (coding for the first tudor domain) with a fusion cassette consisting of β-galactosidase and neomycin resistance gene (β -geo). This results in gene deletion, as transcripts from the mutant allele contains nonsense codons, leading to NMD. The diphtheria toxin A cassette was used for negative selection. The SpeI (S) restriction sites are indicated used for positive clone screening by southern blotting. Note that an additional SpeI site is brought in the targeting vector. (B) Presence of the recombined locus can be detected by Southern blotting with genomic DNA from ES cells or targeted mice. Wild type allele gives a 15.7 kb fragment, while targeted allele generates in a 9.2 kb fragment. (C) Presence of targeted allele is also confirmed by a PCR reaction to amplify a 4.9 kb product (see scheme in A). The primers are anchored on the genomic DNA and the β-geo cassette from the targeting vector. (D) Hematoxylin and eosin staining of 10-day and 20-day old animal testis of the indicated *Tdrd12* genotypes. Spermatogenic defect is hardly apparent in the P10 *Tdrd12* mutant, even though we already noted transposon activation at this early stage (see Fig. 3D). (E) Testis sections were stained for the phosphorylated form of H2AX (γ-H2AX) and DAPI (for DNA). The XY body (sex body) seen in pachytene spermatocytes is visible in control heterozygous *Tdrd12* mutants, but not in homozygous mutants. (F) RT-PCR analysis of genes specifically expressed during various stages of spermatogenesis. Gene normally expressed in haploid round spermatids are not detected in the *Tdrd12* mutant. (G) TUNEL

staining to detect apoptotic cells in P20 (IHC, brown staining) and adult animals (IF, red staining) of indicated genotypes. Note the abundant presence of such cells in the *Tdrd12* mutant. (H) Expressions of retrotransposons in *repro23* mice testes. Expression of both L1 and IAP retrotransposons markedly increased in *repro23*/*repro23* in P10 testis. (I) Unaffected localization of TDRD1 in embryonic testes of indicated *Tdrd12* genotypes.

Fig. S5 Analysis of *Tdrd12* mutants

(A) Promoter CpG DNA methylation (indicated as filled circles) on three imprinted genomic loci was quantified (given in percentages) by bisulfite sequencing. Methylation of imprinted loci is unaffected in *Tdrd12* mutants. (B) Immunoprecipitation of Piwi proteins present in P0 testes of indicated animals. Associated small RNAs were radiolabelled and visualized. Note the absence of MIWI2-bound piRNAs in the *Tdrd12* mutant. This is a repetition of the experiment shown in Fig. 4D. (C-F) Analysis of MILI-associated reads from P0 testes. (C) Genome annotations, (D) nucleotide preference at indicated positions of the reads, (E) mapping to transposon consensus, and (F) mapping to an embryonic piRNA cluster. (G) Pre-pachytene piRNAs are still associated with MILI in the 10-day old (P10) and P14 *Tdrd12* mutants. (H) Electron micrographs showing unaffected presence of electron-dense intermitochondrial cement (arrowheads) in *Tdrd12* mutant fetal testis. Three biological replicates of the mutant were analysed. Mito, mitochondria.

Table S1

All the deep sequencing datasets associated with this study submitted to Gene Expression Omnibus (GEO) under the accession XXXX.

Table S2

List of selected primers used in this study.

SUPPLEMENTAL EXPERIMENTAL PROCEDURES

Clones and antibodies

Mammalian expression constructs

Two isoforms of mouse TDRD12 are identified in the databases: one short form encoding for 407 aa, previously identified as Ecat8 (ES-cell associated transcript 8)(1) and a predicted longer isoform (Acc. No. Q9CWU0) encoding for 1215 aa, which is a C-terminal extension of the shorter isoform. The longer isoform is orthologous to the fly Tdrd12 protein SoYB (2). We confirmed the existence of this longer form in fetal and adult mouse testes total RNA by RT-PCR (Fig. S1A). The full length cDNA for mouse *Tdrd12* was amplified from mouse testes and a mammalian expression construct was generated by inserting the open-reading frame into the pCIneo-HA vector (3). Expression constructs for HA-tagged versions of hAGO2 (3), MILI, MIWI2 and MIWI (4) are already described.

Bombyx Tdrd12 cloning

Using the *Drosophila* Tdrd12 orthologue, SoYb (2) as a query, we mined a *de novo* assembled PolyA+ transcriptome of BmN4 cells (Attie et al., in preparation), and identified a unique cDNA encoding *Bombyx mori* Tdrd12 (BmTdrd12). It is predicted to encode a ~200 kDa protein (1759 aa), which we confirmed by our Western blot analysis of BmN4 cell lysates using the anti-BmTdrd12 antibodies (Fig. S2A). Our efforts to express the full-length protein as an HA-tagged version in BmN4 cells failed. An alignment with *Drosophila* SoYb indicates that ~250 aa at the N-terminus of BmTdrd12 is not conserved. An expression construct lacking 1-259 aa was expressed robustly in BmN4 cells, and is referred in this study as HA-BmTdrd12 (260-1759 aa) (Fig. 2 and Fig. S2B). Based on its interaction with the Piwi protein Siwi and its localization within nuages of transfected BmN4 cells (Fig. 2), we conclude that HA-BmTdrd12 reflects a functional tagged version of the *Bombyx* protein, useful for cell culture studies. Despite the lack of conservation with *Drosophila* proteins, we note that the N-terminal extension of BmTdrd12 (1-259 aa) is conserved in other Lepidopterans like the Monarch butterfly (*Danus plexippus*), displaying 68% similarity and 46% identity over this 259 aa region.

BmTdrd12 protein sequence (the 1-259 aa, in bold, is absent in our HA-BmTdrd12 construct)

MASDYYQVEILHYLNPNLIWVEVLNSPNEISFEQLGVYGILPIDASLDVERPGLKLQRSEDWMPATAILMKNIFQNLEQVWFSPTHIDRRSSIFDNNIHKYGELIIK
KNGVQLYLSKELVKAGLATEDPCQFHQYMSLGKIKTKLSNTETRAVIKNLEEYYRKSSKPKELWQKSVHQNTSIFHAGERLQALTVKNLERHNNRQNIMLLENKLKD
LEQCKGSDEVSLGRGVCRVPSNKSEMVMLTNKRLKNRLELLSKINMKSDATDAVKATKRNFSGDGQRKNFENDFESDDESVKKVSIANTINTSDGSANVVDKLLDEK
QIDNVFNNKKQICYTESTRRNPVKKAACIVYGPPSINIDKLPLKEAPKMTKTVKWTPHVDCDKEASEVSFGDVDSHVKLDVKNLDKFHEIADRIEIEKTIPVDVNIH
KDLYDSMINNKNESESKIMETANLKTEMKNLRKSSILQSKLKQFDKFNVSSNSAASESSTKSSMDSSRISDEDDLSSDDEMSEIMETFKLNLATPKKSEAKHTIDHI
EVNNTKLNANPFKNLDGSKSVFVDKLTSPVLLVHTKRNNKVQPCSLLRDVPFGTSIHVVLRNMGIKHPTRLQTVSWGTILRGLSTFLISPPRSGKTMGYLPAVCRLV
RDFRKESPDSCGPKCIIVCATSKSVSEVERISKMLLGLEDKVFACYSGMDNLSVTTALLNGCDLLICTPKSIVRLLQNDLSVDLRDLTTFVVDDCERISDVYSNEVK
YVLYEIKNMLKNRVNKELKVQIVVASRIWCDFLEPIVLKAPDSVVCIGAFQELILYSKISTTVDFLRPENKIANVLQFIDSVQGPKRTVVVCRADNEVKAVESSLRY
NNRVVFACDNTMNIHDLYNLNVVWGDFEDPTLGPILVCCDSNLVHLNVTDASYLIHYSLPALFSTFCKRFSVLNDNYPSIFKNESRDLKVKVLMDESNVEQLPKILN
FLKRCTENVPKILDEVSEKILNEKDLAKVKDLVPLCDNLLSLGICPDTWNCTERHRIFKECDSPADWIPKNGVVTFQILYFHSAVMYSARLLSNTVDGETTKYPQTY
STLSLKMGMYFSKESSRRLHGIPMVGDVCAVSKKQNFFIRCQVVKIISFYKNGNPNYVVIKLIDEEKFEQSRDIYLYHLPDEFKDMKTYVVQVRLANIQPQDKDITF
SCLAKNELEKIVEKNEDLFMRGHVAMSVGSCIFVDTLEACLDLSSLSETVVRHNFKQELLNAHAVPNPKHLSILEEMCEKSGLIVKAVTNEQVVPKPIPVLPAAQWA
HLEDDLSSVYLASVEDMDKLFVRLVKFESCMKLLNIEINKYVSENTVPLDGSNVGDIVLAKFPDDSMYERARIDHIYSEDKVKCFFVDQGDWRDVSTNDLATITENF
ITQLPFQAIECRLIGIRPFGEQWTEFSTNWFSDHCFEDAKGNLKHLYVKHFTKEKADCTGGHKYGVALIDTYTNEDIIVNQLLIDLNLAKENVDEIAYLSEIKCNKT
VLNNDATVDEEEGSLSGVSEPESNINVPLDKVFLKPPIRSVPLVDSDNETSDSDTWQINRPEDFKALFMRTRPESSKIIPMITANEVQNNADGETSKDTSTILEEKG
QLPEKVKDDELKLSKPKICWSQNKNTVKLKILIAGIEDYKLKIEDRAVAFSANHCDVEYGFKLELYGVVDVNKSRHSNKGQYVLVTMTKLMCRNWLALTKEGDSQKW
IVYDVDTIEASSDEEVYRDDTLEVIKNIHNTNNGSDSEDDDFLDDVS

BmN4 cell expression constructs

Constructs expressing *Bombyx* Siwi and Ago3 were described previously (5). The cDNA encoding BmTdrd12 or its deletions were cloned into the pBEMBL-HA vector to express the following proteins: HA-BmTdrd12 (260-1759 aa), HA-BmTdrd12-A (260-1619 aa), HA-BmTdrd12-B (260-1282 aa), HA-BmTdrd12-C (1407-1759 aa). Introduction of point mutations into predicted ATP-binding or ATP hydrolysis sites of BmTdrd12 was performed by PCR with overlapping primers carrying the required mutations in the respective motifs: ATP-binding (GKT→GAT; K630A) and ATP hydrolysis (DDCE→AACE; D735A, D736A).

Antibodies

For antibody production, cDNAs corresponding to the following amino acids were cloned into the pETM-11 vector (EMBL Protein Expression Facility): *Bombyx* BmTdrd12 (920-1099 aa), mouse MIWI2 (1-212 aa) and mouse TDRD12 (131-398 aa). Insoluble antigens were purified from inclusion bodies and solubilised in 8 M urea. After dilution with adjuvant (1:1), rabbits were injected for polyclonal antibody production. Antibodies were purified with antigen immobilized on filter strips.

Other antibodies used were: anti-MILI mouse monoclonal antibody (13E-3) (4), anti-TDRD1 (6), *Bombyx* Siwi and Ago3 rabbit antibodies (5). The anti-L1ORF1p was a kind gift from Sandra Martin (7). Commercial antibodies were purchased: rabbit anti-HA (Santa Cruz), anti-Myc (EMBL Monocolonal Antibody Core Facility), anti-Actin for detecting *Bombyx* Actin (Santa Cruz; Cat. No. SC-1616-R).

Cell culture experiments

To verify the quality of rabbit polyclonal antibodies to mouse TDRD12, mammalian HEK293T cell cultures (in 6 cm dishes) were transfected (Lipofectamine and Plus Reagent; Invitrogen) with 5 μg of expression plasmids for various proteins. Cell lysates were resolved by 10% SDS-PAGE and proteins analysed by Western blotting to detect tagged proteins with anti-tag antibodies or tested for cross-reactivity with purified anti-TDRD12 antibodies. The purified antibody specifically detected only HA-tagged mouse TDRD12 and no other controls like HA-MILI, MIWI, MIWI2 or Myc-TDRD1.

The BmN4 *Bombyx mori* (silkworm) ovarian cells were transfected (Fugene; Roche) with 2μg of expression plasmids for immunoprecipitation experiments. After 48 h post-transfection, BmN4 cells were lysed in 50 mM Tris-HCl pH 8.0 buffer containing 150 mM NaCl, 0.5% Triton X-100, 0.1% NP-40 and protease inhibitor (Complete protease inhibitor, Roche) in glass tissue homogenizer, and the cell lysate was centrifuged at 16,000 x g for 10min at 4 °C. The supernatant was incubated for 3 h with HA-affinity matrix (Roche) or Protein G Sepharose (GE Healthcare) pre-incubated with antibodies. The immunoprecipitates were separated by SDS-PAGE and analysed by western blot.

Mouse mutants

Generation of the targeted Tdrd12 mutant

To disrupt the in vivo function of *Tdrd12*, we designed a targeting vector to replace exons 3 and 4 (which encode the first tudor domain) with a *β-geo* cassette (β-galactosidase and neomycin resistance fusion gene), by promoter trap selection (Fig. S3A). Homologous recombination removes ~50% of the tudor domain and any mutant transcript would undergo nonsense-mediated decay due to the resulting frame-shift. We PCR-amplified the 5' homology arm (4.4 kb) using KOD plus (Toyobo) with primers 77010-LA-S13341 and 7701010-LA-AS17705. The 3' arm (7 kb) was amplified using the 77010-SA-S19831 and 77010-AS26839(X) primers. The IRES *β-geo* cassette was inserted between the two PCR-amplified homology arms. For negative selection, the diphtheria toxin-A cassette was placed downstream of the 3' arm. The targeting vector was linearized with Not I and

introduced into RF8 ES cells by electroporation. We identified clones with homologous recombination by PCR. Primer 77010-LA-S12295 was designed to bind to sequence upstream of the 5' arm, and the antisense primer (β-*geo* screening AS2) recognizes the *β-geo* cassette, yielding a 4.9 kb fragment for the targeted allele. PCR-positive clones were genotyped by Southern blotting with a 3' probe (523 bp) which was amplified using primers m77010gU28402 and m77010gL28925. ES cell genomic DNA was extracted with Puregene Cell Lysis Solution (Gentra systems), digested with SpeI, separated on a 0.8% agarose gel, and transferred to a nylon membrane. The Southern probe detected 15.7 kb and 9.2 kb fragments from the wild-type and targeted alleles, respectively (Fig. S3B). Presence of the targeted allele was further confirmed by detection of a 4.9 kb PCR fragment (Fig. S3C). The targeted ES cells were then used to generate mutant mice by standard procedures. Animals were maintained in C57BL/6;129S4/SvJae mixed genetic background.

Once correctly targeted clones were identified, cells and mice were genotyped using a three-primer PCR assay. The common primer m77010-gU17547 was designed to anneal to intron 2 of both the wild-type and targeted loci. Primer m77010-gL18297 binds to intron 3 and together with primer m77010-gU17547 amplifies a 774 bp wild-type fragment. The *β-geo* screening AS2 primer amplifies a 250 bp fragment from the targeted allele in combination with primer m77010-gU17547. All primers used for creation and analysis of the targeted *Tdrd12* mutant are listed in Table S2.

Generation and characterization of ENU-induced mutant mouse for Tdrd12

The *repro23* mutant mice were produced by ENU-induced mutagenesis in the ReproGenomics Program of The Jackson Laboratory (Asano et al., 2009). A total of 587 male F_2 mice were obtained by intercross of heterozygous (+/*repro23*) F_1 mice, derived from the cross between *repro23*/*repro23* homozygous female and JF1/Ms (+/+) male mice. The *repro23* locus has previously been mapped on a 2.2-Mb region of mouse chromosome 7 (Asano et al., 2009). By genotyping seven microsatellite markers on this region, we found no recombination between the *repro23* locus and a microsatellite marker *D7Mit78*, while at least one recombination was found between the *repro23* locus and the remaining 6 microsatellite marker. Therefore, the *repro23* critical region was narrowed down to the 0.9-Mb interval between *D7Mit225* and *D7Mok1*.

Genomic DNA and cDNA synthesized from testis RNA of the mutant and normal mice were used for sequencing of the 13 candidate genes in the 0.9-Mb critical region. The PCR and RT-PCR products covering entire coding regions of these genes were sequenced by using ABI PRISM 310 Genetic Analyzer (Applied Biosystems). By comparing the sequences between normal and *repro23*/*repro23* mice, a nucleotide substitution of C to A resulting in nonsense mutation was found in exon 8 of the *Tdrd12* gene. No other mutation was found in the remaining genes.

Total RNA was isolated from testes using TRIzol regent (Invitrogen), reverse-transcribed into cDNA using oligo dT primers and PrimeScript RTase (Takara), and subjected for PCR reactions using primers for *Tdrd12* gene (TGTTCGAGGTCCTGGTGCTG and GCTTCCACTTGGGTAGTTGCTC)

or L1 (GGCGAAAGGCAAACGTAAGA and GGAGTGCTGCGTTCTGATGA) and IAP (AACCAATGCTAATTTCACCTTGGT and GCCAATCAGCAGGCGTTAGT) retrotransposones.

Immunoprecipitations and nucleic acid analyses

Immunoprecipitations, and 5'-end labelling were as previously described (4). Germ cells were purified from testes and bisulfite conversion of the genomic DNA and bisulfite analyses were performed as reported (8).

Northern blot analysis of transposon expression

Total RNA was extracted from testes of wild type, heterozygous and homozygous *Tdrd12* mutant mice using TRI reagent according to manufacturer guide (MRC Inc, Cat. No. TR 118) and treated with DNaseI (Fermentas). Approximately 10ug of DNaseI-treated RNA was analysed on denaturing formamide agarose gel and transferred onto Nylon membrane (Amersham, Hybond N+) through capillary transfer for 16 hours in 20x SSC solution (For 1 liter : 175 g NaCl, 88,2 g Na Citrate dehydrate). After transfer was complete, membrane was taken out and UV crosslinked with 120 mJ/cm2 in Stratagene "cross linker". Crosslinked membrane was washed with 2XSSC once. Prehybridization was done at least for 2 hours in Church buffer (0,25 M NaPhospate buffer, pH 7,2 1 mM EDTA 1% (w/v) BSA 7% w/v) SDS, Filter solution) at 65°C.

Radiolabelled L1 probe was prepared from LINE1 DNA fragment (515bp-1680bp, GeneBank accession number M13002) (9) using Random prime DNA labeling kit (Roche, Cat No 1004760001). Radiolabelled IAP probe were similarly prepared from the IAP DNA (GeneBank accession number AF 303453). Probes were denatured at 95°C for 5 minutes and hybridized with membrane in Church buffer at 65°C overnight with continuous mixing. Next day washing was performed at 65°C as followed: twice 15 minutes each with buffer-1 (2xSSC, O.1% SDS), twice 15 minutes each with buffer-2 (0.2xSSC, 0.1%SDS) and finally with 0.1xSSC at room temperature for 5 minutes. Membrane was wrapped in plastic film and exposed to Phosphor Imaging screen and scanned with typhoon scanner (GE Healthcare).

Immunofluorescence

Hematoxylin and eosin staining was performed on paraffin sections of testes samples. Immunofluorescence analysis was performed on O.C.T (Tissue-Tek Cryo-OCT compound, Fischer Scientific) embedded testes cryosections. After incubation with primary antibodies, slides were washed, and further incubated with Alexa 488 or 555-coupled secondary antibodies (Invitrogen). Samples were then examined by fluorescence microscopy (Olympus BX61) and images captured using CCD (Olympus DP70).

BmN4 cells were grown on coverslips and endogenous Piwi proteins or transfected proteins were detected as reported previously (5). Confocal images of the indirect fluorescence were recorded using a Leica TCS SP2 AOBS inverted microscope.

Small RNA libraries and bioinformatics

Small RNA libraries from immunoprecipitated RNAs were prepared by using the NEB kit (NEBNext® Multiplex Small RNA Library Prep Set for Illumina® (1–12), Cat no:E7300). For total small RNA libraries from P0 testes of *Tdrd12*$^{+/-}$ and *Tdrd12*$^{-/-}$ animals, small RNAs (~14-40 nt) were gel purified by urea-PAGE and library was prepared as above. Small RNA libraries were sequenced for 50 cycles with Illumina Genome Analyzer IIx (EMBL Gene core facility).

After sequencing, reads were processed to remove adapter sequences, followed by sorting based on the barcode information. These reads were then mapped to the mouse (July 2007, NCBI37/mm9 assembly) or *Bombyx mori* genome (10). Only perfectly mapping reads were retained for further analysis. Genome annotations were extracted based on those defined by Entrez. For plotting repeat small RNA density, reads were mapped to transposon consensus allowing up to a maximum of 3 mismatches as previously described (11). Density plots were displayed after normalization of all libraries to 1 million reads.

The following proteins were used in the sequence alignment showing aromatic cage residues in tudor domains (Fig. 1C): human Staphylococcal nuclease domain-containing 1 (SND1) (GI:77404396); *Drosophila* Tudor (GI:19550189); mouse TDRD1 (GI:268607546); *Drosophila* CG31755 (SoYb) (GI:386769395), CG11133 (BoYb) (GI:24668815); *Bombyx mori* Tdrd12 (see above); and mouse TDRD12 (Acc. No. Q9CWU0).

SUPPLEMENTAL REFERENCES

1. Mitsui K, *et al.* (2003) The homeoprotein Nanog is required for maintenance of pluripotency in mouse epiblast and ES cells. *Cell* 113(5):631-642.
2. Handler D, *et al.* (2011) A systematic analysis of Drosophila TUDOR domain-containing proteins identifies Vreteno and the Tdrd12 family as essential primary piRNA pathway factors. *Embo J* 30(19):3977-3993.
3. Pillai RS, Artus CG, & Filipowicz W (2004) Tethering of human Ago proteins to mRNA mimics the miRNA-mediated repression of protein synthesis. *Rna* 10(10):1518-1525.
4. Reuter M, *et al.* (2009) Loss of the Mili-interacting Tudor domain-containing protein-1 activates transposons and alters the Mili-associated small RNA profile. *Nat Struct Mol Biol* 16(6):639-646.
5. Xiol J, *et al.* (2012) A Role for Fkbp6 and the Chaperone Machinery in piRNA Amplification and Transposon Silencing. *Mol Cell* 47(6):970-979.
6. Chuma S, *et al.* (2006) Tdrd1/Mtr-1, a tudor-related gene, is essential for male germ-cell differentiation and nuage/germinal granule formation in mice. *Proc Natl Acad Sci U S A* 103(43):15894-15899.
7. Branciforte D & Martin SL (1994) Developmental and cell type specificity of LINE-1 expression in mouse testis: implications for transposition. *Mol Cell Biol* 14(4):2584-2592.

8. Kato Y*, et al.* (2007) Role of the Dnmt3 family in de novo methylation of imprinted and repetitive sequences during male germ cell development in the mouse. *Hum Mol Genet* 16(19):2272-2280.
9. Soper SF*, et al.* (2008) Mouse maelstrom, a component of nuage, is essential for spermatogenesis and transposon repression in meiosis. *Dev Cell* 15(2):285-297.
10. Wang J*, et al.* (2005) SilkDB: a knowledgebase for silkworm biology and genomics. *Nucleic Acids Res* 33(Database issue):D399-402.
11. Olson AJ, Brennecke J, Aravin AA, Hannon GJ, & Sachidanandam R (2008) Analysis of large-scale sequencing of small RNAs. *Pacific Symposium on Biocomputing*:126-136.

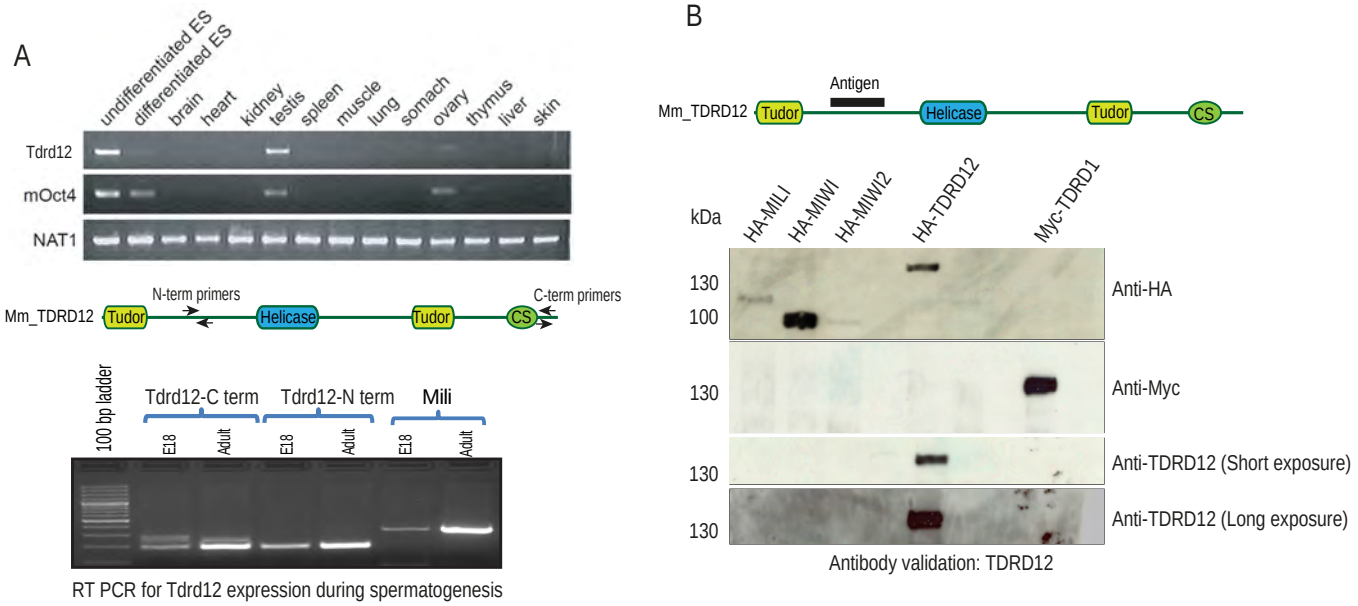
A
undifferentiated ES
differentiated ES
brain
heart
kidney
testis
spleen
muscle
lung
somach
ovary
thymus
liver
skin
Tdrd12
mOct4
NAT1
N-term primers
C-term primers
Mm_TDRD12
Tudor
Helicase
Tudor
CS
100 bp ladder
Tdrd12-C term
Tdrd12-N term
Mili
E18
Adult
E18
Adult
E18
Adult
RT PCR for Tdrd12 expression during spermatogenesis
B
Antigen
Mm_TDRD12
Tudor
Helicase
Tudor
CS
kDa
HA-MILI
HA-MIWI
HA-MIWI2
HA-TDRD12
Myc-TDRD1
130
100
Anti-HA
130
Anti-Myc
130
Anti-TDRD12 (Short exposure)
130
Anti-TDRD12 (Long exposure)
Antibody validation: TDRD12
C
IP
kDa
Input
Beads
TDRD12
TDRD12 + RNase A
MILI
100
MILI
130
TDRD12
130
TDRD1
Western blot (Adult testes)
D
M
1
2
3
4
5
6
7
8
9
Elution franctions
Tud2
His-tagged 2nd Tudor domain (Tud2) of TDRD12
E
Time (min)
Kd ~ 350-500 µM
[R-me2sym]/[Tud3-TDRD1]
[R-me2sym]/[Tud2-TDRD12]
[R-me]/[Tud2-TDRD12]
[R]/[Tud2-TDRD12]

Fig. S1

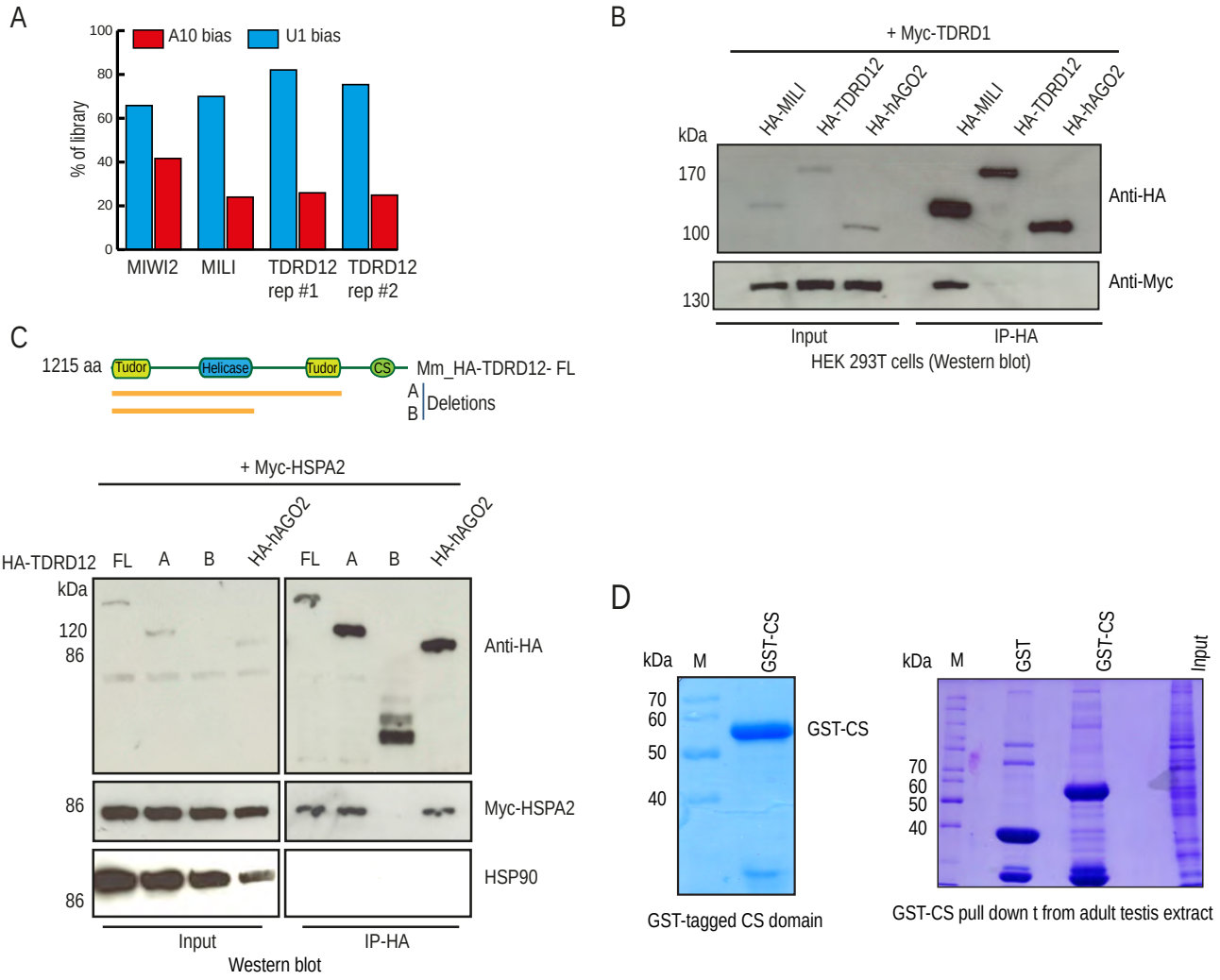
A
A10 bias
U1 bias
% of library
MIWI2
MILI
TDRD12 rep #1
TDRD12 rep #2
B
+ Myc-TDRD1
HA-MILI
HA-TDRD12
HA-hAGO2
kDa
170
100
130
Anti-HA
Anti-Myc
Input
IP-HA
HEK 293T cells (Western blot)
C
1215 aa
Tudor
Helicase
Tudor
CS
Mm_HA-TDRD12- FL
A
B
Deletions
+ Myc-HSPA2
HA-TDRD12
FL
A
B
HA-hAGO2
kDa
120
86
Anti-HA
Myc-HSPA2
HSP90
Input
IP-HA
Western blot
D
kDa
M
GST-CS
70
60
50
40
GST-CS
GST-tagged CS domain
GST
Input
GST-CS pull down t from adult testis extract

Fig. S2

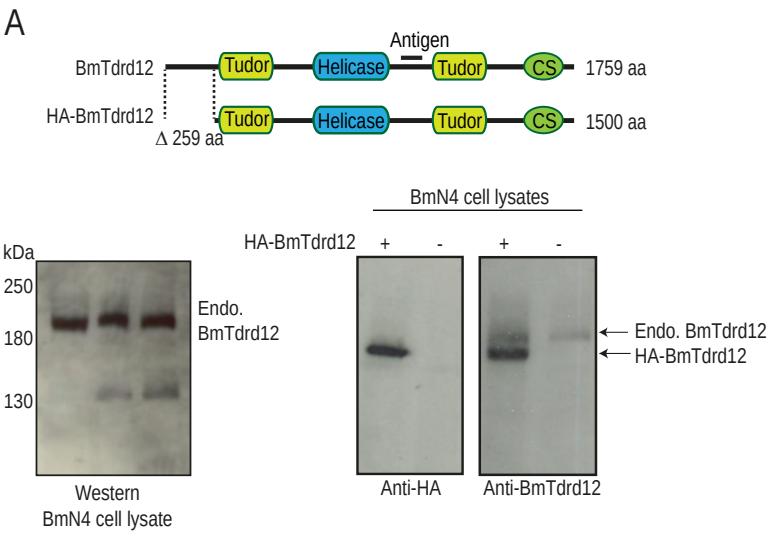
A
Antigen
BmTdrd12
Tudor
Helicase
Tudor
CS
1759 aa
HA-BmTdrd12
Tudor
Helicase
Tudor
CS
1500 aa
Δ 259 aa
BmN4 cell lysates
HA-BmTdrd12 + - + -
kDa
250
180
130
Endo.
BmTdrd12
Endo. BmTdrd12
HA-BmTdrd12
Western
BmN4 cell lysate
Anti-HA
Anti-BmTdrd12

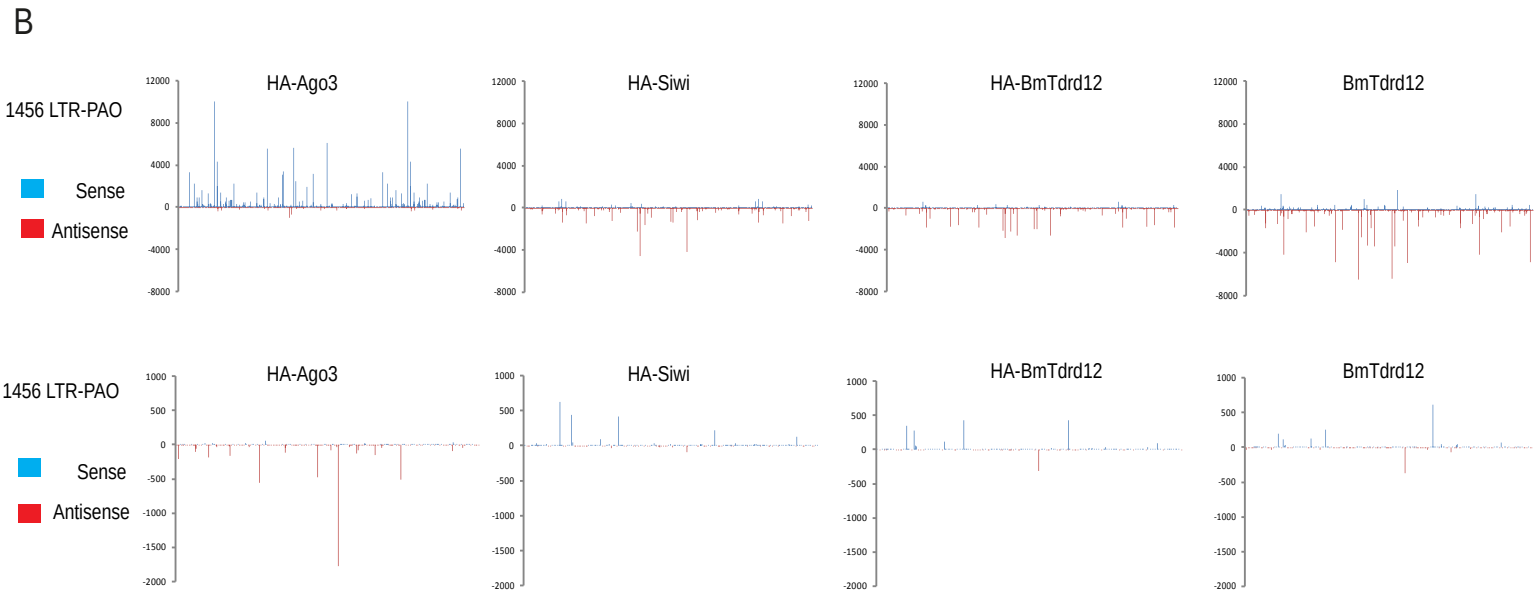
B
1456 LTR-PAO
Sense
Antisense
HA-Ago3
HA-Siwi
HA-BmTdrd12
BmTdrd12
12000
8000
4000
0
-4000
-8000
1456 LTR-PAO
Sense
Antisense
HA-Ago3
HA-Siwi
HA-BmTdrd12
BmTdrd12
1000
500
0
-500
-1000
-1500
-2000

Fig. S3

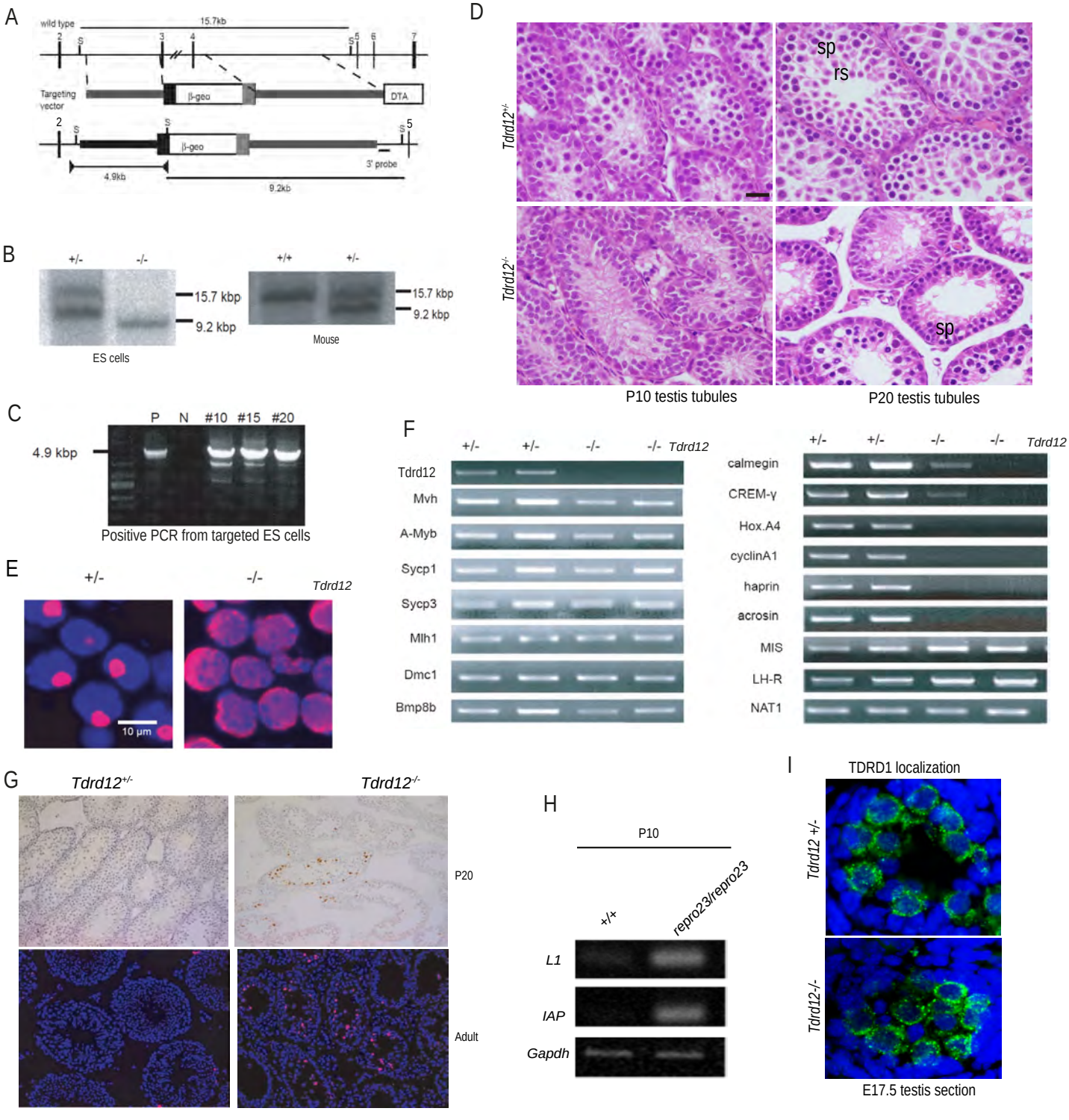
A
wild type
15.7kb
Targeting vector
β-geo
DTA
4.9kb
9.2kb
3' probe
B
+/-
-/-
+/+
15.7 kbp
9.2 kbp
ES cells
Mouse
C
P
N
#10
#15
#20
4.9 kbp
Positive PCR from targeted ES cells
D
Tdrd12+/-
Tdrd12-/-
sp
rs
P10 testis tubules
P20 testis tubules
E
+/-
-/-
Tdrd12
10 µm
F
Tdrd12
Mvh
A-Myb
Sycp1
Sycp3
Mlh1
Dmc1
Bmp8b
calmegin
CREM-γ
Hox.A4
cyclinA1
haprin
acrosin
MIS
LH-R
NAT1
G
Tdrd12+/-
Tdrd12-/-
P20
Adult
H
P10
+/+
repro23/repro23
L1
IAP
Gapdh
I
TDRD1 localization
Tdrd12 +/-
Tdrd12-/-
E17.5 testis section

Fig. S4

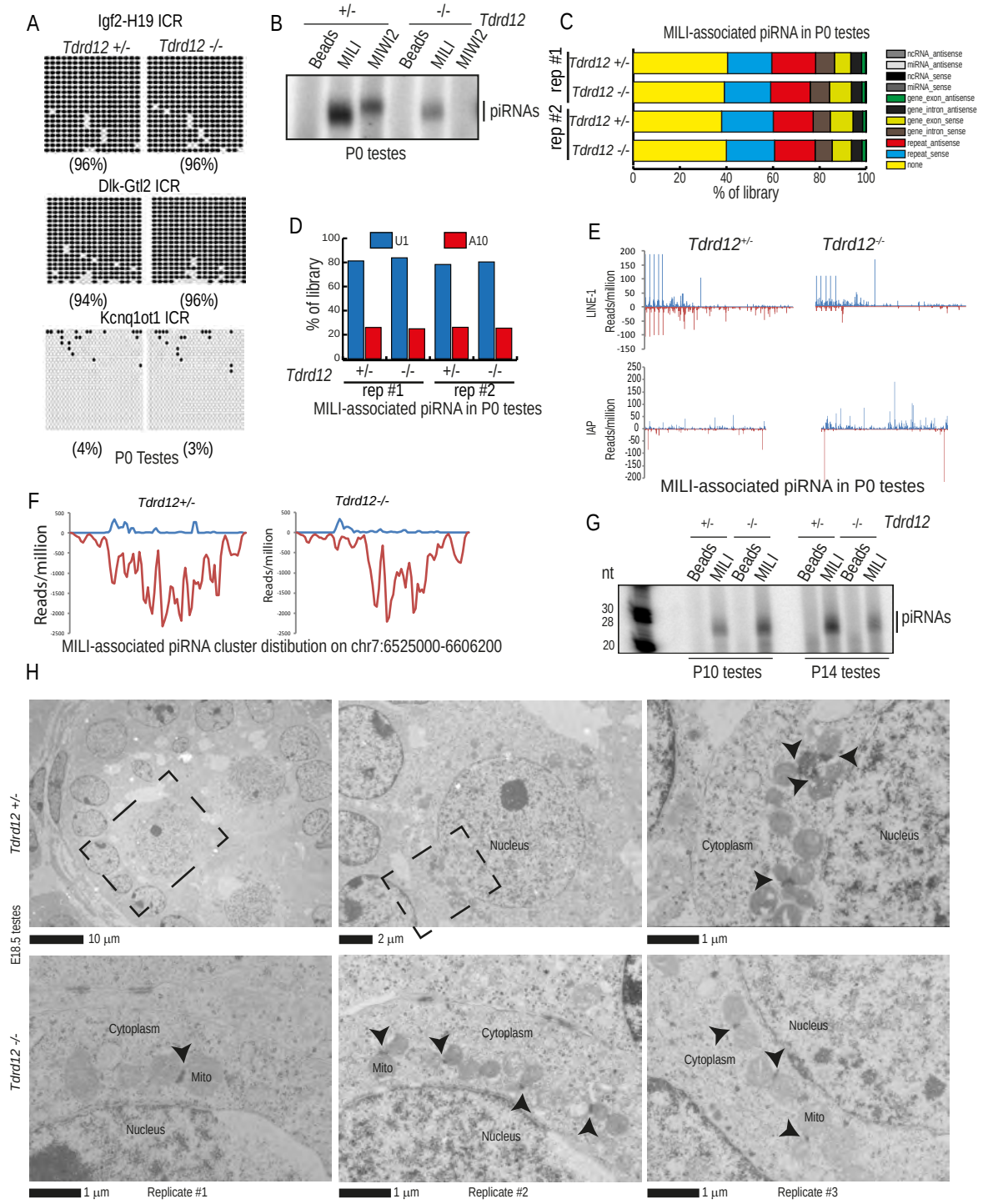
A
Igf2-H19 ICR
Tdrd12 +/-
Tdrd12 -/-
(96%)
(96%)
Dlk-Gtl2 ICR
(94%)
(96%)
Kcnq1ot1 ICR
(4%)
P0 Testes
(3%)
B
+/-
-/-
Tdrd12
Beads
MILI
MIWI2
Beads
MILI
MIWI2
piRNAs
P0 testes
C
MILI-associated piRNA in P0 testes
rep #1
rep #2
Tdrd12 +/-
Tdrd12 -/-
Tdrd12 +/-
Tdrd12 -/-
ncRNA_antisense
miRNA_antisense
ncRNA_sense
miRNA_sense
gene_exon_antisense
gene_intron_antisense
gene_exon_sense
gene_intron_sense
repeat_antisense
repeat_sense
none
0
20
40
60
80
100
% of library
D
U1
A10
% of library
Tdrd12
+/-
-/-
+/-
-/-
rep #1
rep #2
MILI-associated piRNA in P0 testes
E
Tdrd12+/-
Tdrd12-/-
LINE-1
Reads/million
IAP
Reads/million
MILI-associated piRNA in P0 testes
F
Tdrd12+/-
Tdrd12-/-
Reads/million
Reads/million
MILI-associated piRNA cluster distibution on chr7:6525000-6606200
G
+/-
-/-
+/-
-/-
Tdrd12
Beads
MILI
Beads
MILI
Beads
MILI
Beads
MILI
nt
30
28
20
piRNAs
P10 testes
P14 testes
H
Tdrd12 +/-
E18.5 testes
Tdrd12 -/-
Nucleus
Cytoplasm
Nucleus
10 μm
2 μm
1 μm
Cytoplasm
Mito
Nucleus
Cytoplasm
Mito
Nucleus
Nucleus
Cytoplasm
Mito
1 μm
Replicate #1
1 μm
Replicate #2
1 μm
Replicate #3

Fig. S5

Table S1: List of all deep sequencing datasets used in this study

Library	Organism	Age	Genotype	Mapped reads
MILI IP # rep1	Mouse	P0	*Tdrd12* +/-	16473692
MILI IP # rep1	Mouse	P0	*Tdrd12* -/-	15024728
MILI IP # rep2	Mouse	P0	*Tdrd12* +/-	19246231
MILI IP # rep2	Mouse	P0	*Tdrd12* -/-	15722298
Total small RNA (14-40 nt)	Mouse	P0	*Tdrd12* +/-	12393343
Total small RNA (14-40 nt)	Mouse	P0	*Tdrd12* -/-	16113332
MILI IP	Mouse	E18	wild type	16549061
MIWI2 IP	Mouse	E18	wild type	12590475
TDRD12 IP # rep1	Mouse	E18	wild type	9071424
TDRD12 IP # rep2	Mouse	E18	wild type	10209745
HA-Tdrd12 IP	*Bombyx* cell line, Bmn4	N/A	N/A	10213582
BmTDRD12 IP (endogenous)	*Bombyx* cell line, Bmn4	N/A	N/A	12018857

Table S2: List of primers used for characterizing Tdrd12 targeted mouse mutant	
MvhVg2	CCA AAA GTG ACA TAT ATA CCC
MvhVas3	TTG GTT GAT CAG TTC TCG AG
CREM Upper	GAT TGA AGA AGA AAA ATC AGA
CREM Lower	CAT GCT GTA ATC AGT TCA TAG
Dmc1Upper	TTC GTA CTG GAA AAA CTC AGC TGT ATC
Dmc1Lower	CTT GGC TGC GAC ATA ATC AAG TAG CTC C
HoxA4Upper	TGA GCG CTC TCG AAC CGC CTA TAC C
HoxA4Lower	GAT GGT GGT GTG GGC TGT GAG TTT G
Mlh1Upper	AGG AGC TGA TGC TGA GGC
Mlh1Lowe	TTT CAT CTT GTC ACC CGA TG
Sycp-1Upper	ATG GAG AAG CAA AAG CCC TTC
Sycp-1Lower	TTT CTG CTT CAG TTC AGA TTC
CyclinA1Upper	ATG CAT CGC CAG AGC TCC AAG AG
CyclinA1Lower	GGA AGT GGA GAT CTG ACT TGA GC
Sycp-3Upper	GGT GGA AGA AAG CAT TCT GG
Sycp-3Lower	CAG CTC CAA ATT TTT CCA GC
A-MybUpper	AAG AAG TTG GTT GAA CAA CAC GG
A-MybLower	AGG AAG TAA CTT AGC AAT CTC GG
CalmeginUpper	ATA TGC GTT TCC AGG GTG TTG GAC
CalmeginLower	GTA TGC ACC TCC ACA ATC AAT ACC
NAT1-U10	GAGTCGGAGCTCTATGGAGGTGG
NAT1-L21	GCCCGAAGAAGCACTGAAACGAGAA
Bmp-8bUpper	CGC AAC ATG GTA GTC CAG GC
Bmp-8bLower	GGA TAC TGA AGA GCC TGA GC
MIS-S	TTG GTG CTA ACC GTG GAC TT
MIS-AS	GCA GAG CAC GAA CCA AGC GA
m77010-U362	CTG GTG CAG GGC TCT GAT TAA GTC
m77010-L1148	TTT ACA CAG CCG TTC TTC TCG TCA
Acrosin-S	CGG AGT CTA CAC AGC CAC CT
Acrosin-AS	GCA TGA GTG ATG AGG AGG TT
Haprin-S	CCA GAA CAT GAG ACA GAG AG
Haprin-AS	AGC AAC TTC CTG AGC ATA CC
LH-R-S	TGC AAC CTC CTC AAT CTG TC
LH-R-AS	AGC GTG GCA ACC AGT AGG CT
m77010-gU17547	ACT GTT GCT AAT GGG AGC TAC TGT
m77010-gL18297	GGG CAG TAT CTT TCC TGA GTC ATA
bGeo-screening-AS6	GCG GAA TTC TCT AGA GTC CAG ATC
77010-LA-S13341	AGG ATG GTT AGG CAA GGT TCT CTT ACT C
77010-LA-AS17705	GCA CTT CAG CTC CTG GCA GTA CAC CAC A
77010-SA-S19831	TGT GAA GAC ATC CAG CGC AGG TTG ACT T
77010-AS26839(X)	GGC TCG AGT CCA CCT CAT ACC TGA
m77010-gU28402	GGG GAA GAT TTT TAT TGT TGC TA
m77010-gL28925	AAG AGT TGT AGG CAC TGC AAA CAC
bgeo-screening-AS2	GACCTTGCATTCCTTTGGCGAGAG
Primer for cloning *Tdrd12* antigen	
RP oligo 820	CATGCCATGGAGAAGCCTGTGACATTGCACATTG
RP oligo 821	ATTCTTATGCGGCCGCTTACTTCTTCAGGTCTGCCGACAG

Primer for cloning Tudor domain of *Tdrd12*	
RR oligo258	CATGCCATGGGTTTCGAGGTCCTGGTGCTG
RR oligo259	ATTCTTATGCGGCCGCTCACCCCATTGGTGACACATAATAAGC
RR oligo261	CATGCCATGGGACACATTAGGGTAATACCTTTTTACAT
RR oligo262	ATTCTTATGCGGCCGCTCAGTCAGCTGGCTTAACCCTACAA
Primers for *Tdrd12* RT PCR	
RR oligo331	CTTCAGTGCCTGGGTAGGAG
RR oligo332	TCCTCCCAGTGGTCAAAGTC
RR oligo333	TGTGTACTGGCCAACCAAAA
RR oligo334	CTGAGGTCCCATCAGCTCTC